

1 The Eurasian Arctic Ocean along the MOSAiC drift in
2 2019–2020: An interdisciplinary perspective on physical
3 properties and processes

4 Kirstin Schulz^{1,2,*}, Zoe Koenig^{3,4,5}, Morven Muilwijk⁴, Dorothea Bauch^{6,7},
5 Clara J. M. Hoppe², Elise S. Droste^{2,8}, Mario Hoppmann², Emelia J.
6 Chamberlain^{9,10}, Georgi Laukert^{11,10}, Tim Stanton¹², Alejandra Quintanilla-
7 Zurita², Ilker Fer⁵, Céline Heuzé¹³, Salar Karam¹³, Sebastian Mieruch-Schnülle²,
8 Till M. Baumann^{5,14}, Myriel Vredenburg², Sandra Tippenhauer², Mats A.
9 Granskog⁴

10 ¹Oden Institute for Computational Engineering and Sciences, The University of Texas at Austin,
11 Austin, TX, United States

12 ²Alfred Wegener Institute Helmholtz Centre for Polar and Marine Research, Bremerhaven,
13 Germany

14 ³UiT The Arctic University of Norway, Tromsø, Norway

15 ⁴Norwegian Polar Institute, Fram Centre, Tromsø, Norway

16 ⁵Geophysical Institute, University of Bergen and Bjerknes Centre for Climate Research, Bergen,
17 Norway

18 ⁶Leibniz-Laboratory, University of Kiel (CAU), Kiel, Germany

19 ⁷GEOMAR Helmholtz Centre for Ocean Research, Kiel, Germany

20 ⁸School of Environmental Sciences, University of East Anglia, Norwich, United Kingdom

21 ⁹Scripps Institution of Oceanography, University of California, San Diego, CA, United States

22 ¹⁰Woods Hole Oceanographic Institution, Woods Hole, MA, United States

23 ¹¹School of Earth Sciences, University of Bristol, Bristol, United Kingdom

24 ¹²Oceanography Department, Naval Postgraduate School, Monterey, CA, United States

25 ¹³Department of Earth Sciences, University of Gothenburg, Gothenburg, Sweden

26 ¹⁴Institute of Marine Research, Bergen, Norway

27 **This manuscript has been accepted for publication in *Elementa: Science***
28 **of the Anthropocene 5/13/2024. One published, the final version of this**
29 **manuscript will be available via the “Peer reviewed Publication DOI” link**
30 **on the right-hand side of this page and will be available open-access on the**
31 **publisher’s website. For any question, contact Kirstin Schulz.**

32 Abstract

33 The Multidisciplinary drifting Observatory for the Study of Arctic Climate (MO-
34 SAiC, 2019–2020), a year-long drift with the Arctic sea ice, has provided the
35 scientific community with an unprecedented, multidisciplinary dataset from the
36 Eurasian Arctic Ocean, covering high atmosphere to deep ocean across all sea-
37 sons. However, the heterogeneity of data and the superposition of spatial and tem-
38 poral variability, intrinsic to a drift campaign, complicate the interpretation of
39 observations. In this study, we have compiled a quality-controlled physical hydro-
40 graphic dataset with best spatio-temporal coverage and derived core parameters,
41 including the mixed layer depth, heat fluxes over key layers, and friction veloc-
42 ity. We provide a comprehensive and accessible overview of the ocean conditions
43 encountered along the MOSAiC drift, discuss their interdisciplinary implications,
44 and compare common ocean climatologies to these new data. Our results indi-
45 cate that, for the most part, ocean variability was dominated by regional rather
46 than seasonal signals, carrying potentially strong implications for ocean biogeo-
47 chemistry, ecology, sea ice, and even atmospheric conditions. Near-surface ocean
48 properties were strongly influenced by the relative position of sampling, within
49 or outside the river-water influenced Transpolar Drift, and seasonal warming and
50 meltwater input. Ventilation down to the Atlantic Water layer in the Nansen Basin
51 allowed for a stronger connectivity between subsurface heat and the sea ice and
52 surface ocean via elevated upward heat fluxes. The Yermak Plateau and Fram
53 Strait regions were characterized by heterogeneous water mass distributions, en-
54 ergetic ocean currents, and stronger lateral gradients in surface water properties in
55 frontal regions. Together with the presented results and core parameters, we offer
56 context for interdisciplinary research, fostering an improved understanding of the
57 complex, coupled Arctic System.

58 1. Introduction

59 To a large extent, the Arctic Ocean has been historically inaccessible due to its
60 perennial ice cover, resulting in limited data availability, particularly during win-
61 ter. With global warming triggering rapid transformations in the Arctic (Rantanen
62 et al., 2022), a better understanding of processes in the Arctic Ocean and its role
63 in the coupled climate system is urgently needed to accurately predict the effects
64 of a changing climate. Ongoing changes in the Arctic Ocean include declining
65 sea ice cover and longer open water seasons (e.g., Stroeve et al., 2008; Kwok,
66 2018; Kim et al., 2023), Atlantification, i.e., the progression of conditions typi-
67 cal for the North Atlantic farther into the Arctic Ocean (Polyakov et al., 2017),

68 a weakening upper ocean stratification, enhanced vertical mixing and transport
69 (Polyakov et al., 2020b,a; Schulz et al., 2022a), increased primary productivity
70 (Arrigo and van Dijken, 2015), and changes in the Arctic ecosystem composition
71 (Gordó-Vilaseca et al., 2023). These changes are observed primarily in the East-
72 ern Arctic, while conditions in the Western Arctic exhibit less clear patterns, e.g.,
73 no conclusive evidence of increased mixing (Dosser et al., 2021; Fine and Cole,
74 2022), or even show opposite trends, e.g., increased stratification by freshwater
75 accumulation in the Beaufort Gyre (Timmermans and Toole, 2023).

76 The Multidisciplinary drifting Observatory for the Study of Arctic Climate
77 (MOSAiC) was a year-long (2019–2020) drift campaign with the aim to improve
78 our process-level understanding of the coupled Arctic System (Rabe et al., 2022;
79 Shupe et al., 2022; Nicolaus et al., 2022; Fong et al., 2023). A large number of
80 interdisciplinary efforts in MOSAiC involved physical oceanography parameters,
81 such as ocean temperature and salinity or current velocity. Examples include ef-
82 forts to calculate the solubility of gases, to determine the origin of water masses
83 that transport tracers and organisms, to quantify the contribution of oceanic heat
84 to sea ice formation and melting, and to constrain the variability in ice-nucleating
85 particles of marine origin. In addition, the modeling community requires updated
86 oceanic boundary conditions and core parameters for model validation (Heuzé
87 et al., 2023b), while climatological datasets, which are often crucial components
88 in modeling frameworks, need ground-truthing to current conditions. However,
89 the diversity of oceanographic equipment used during MOSAiC and the resulting
90 scattered datasets at various levels of processing and documentation hinder easy
91 access to and utilization of these data, especially for non-physical oceanographers
92 and scientists not involved in the field campaign. In addition, the design of MO-
93 SAiC as a drifting platform complicates the interpretation of oceanographic mea-
94 surements. Superimposed on the annual cycle is the regionality along the more
95 than 3500 km long drift track across the Eurasian basin (Figure 1a; Rabe et al.,
96 2022). These challenges might lead to an inconsistent usage and interpretation of
97 the oceanographic data and hinder the inter-comparability of individual studies in
98 the future.

99 In this study, we have compiled an accessible and quality-controlled dataset
100 of hydrographic profiles at the highest possible temporal resolution along the drift
101 and provide derived core parameters (Schulz et al., 2023b), including an inter-
102 active data interface (Mieruch, 2023) in the online Ocean Data View webODV
103 (Mieruch and Schlitzer, 2023), which can be used consistently in future disci-
104 plinary and interdisciplinary studies. Based on this dataset, we present a com-
105 prehensive overview of ocean conditions during the MOSAiC drift, discuss their

106 effect on the coupled system and, to the extent possible, discriminate between
107 spatial and temporal signals. This description of the state of the Eurasian Arctic
108 Ocean in 2019–2020 and the comparison of commonly used climatological
109 datasets to these modern data will also aid the evaluation of ocean models.

110 The structure of this paper is as follows. In Section 2, we provide a brief
111 overview of the methods and instrumentation used in this study (more detailed
112 information is available in Text S1). Section 3 describes the geography along the
113 drift track of MOSAiC, and in Section 4 we summarize the water column structure
114 and water mass distribution. Section 5 then focuses on dynamic features, such as
115 surface and tidal current variability and eddies. Parameters related to ocean mix-
116 ing, such as the vertical diffusivity and heat fluxes, are presented in Section 6. In
117 Section 7, we compare MOSAiC results to existing climatologies. In the Section 8,
118 we contextualize the MOSAiC data by comparing them to previous findings and
119 discuss the implications of these results for other scientific disciplines. Finally,
120 Section 9 summarizes the main findings and concludes the paper.

121 2. Methods and instrumentation

122 The MOSAiC drift started in September 2019, using the icebreaker RV *Polarstern*
123 (Knust, 2017) as a drifting platform frozen into the Arctic sea ice, with measure-
124 ments conducted from the same ice floe and surrounding sites during five cruise
125 legs. On-site sampling was interrupted from May 15 to June 27, 2020, due to the
126 unavailability of a second icebreaker during the COVID-19 pandemic to perform
127 personnel exchange and resupply, but resumed on the same floe. At the end of
128 July, the floe disintegrated in the marginal ice zone in Fram Strait; after reloca-
129 tion north, a second floe was chosen close to the previous drift track to sample the
130 freeze-up period. In the following, we briefly summarize the different datasets and
131 methods used in this study. More details can be found in Text S1, and an overview
132 of the sampling locations is presented in Rabe et al. (2022).

133 We obtained water depths from three different sources: the *Polarstern*
134 echosounder, the combined altimeter and depth readings from the deep casts of the
135 ship-based conductivity-temperature-depth (CTD) profiling system and the Inter-
136 national Bathymetric Chart of the Arctic Ocean (IBCAO) v4.2 bathymetric dataset
137 (Jakobsson et al., 2020). Drift track and speed were obtained from the *Polarstern*
138 navigation records and complemented with data from a GPS buoy (“CO1”) that
139 remained on the floe when sampling was interrupted in spring. From the drift ve-
140 locity, we calculated the ice friction velocity u_* based on the Rossby similarity
141 (see Text S1), as done in Kawaguchi et al. (2022).

142 In total, a set of 2,434 vertical temperature and salinity profiles were com-
 143 piled, including data from the microstructure profiler (MSS) operated at Ocean
 144 City, i.e., a sampling site in the Central Observatory (CO) on the main floe (1,665
 145 profiles, 0–350 m; Schulz et al., 2023c), the Ocean City CTD (121 profiles, down
 146 to maximum 1000 m; Tippenhauer et al., 2023a) and the *Polarstern* CTD (134
 147 profiles, excluding those during transit; Tippenhauer et al., 2023b). During the
 148 drift interruption and on days without any MSS or CTD casts, we used profiles
 149 from the ice-tethered profilers ITP94 and ITP111 (428 profiles, down to 1000 m
 150 depth; Toole and Krishfield, 2016) and daily mean data at five discrete depths
 151 (10 m, 25 m, 50 m, 75 m, 100 m) from a CTD chain on Pacific Gyre buoy 2019O4
 152 (86 days; Hoppmann et al., 2022), all deployed near the CO at the start of the drift.
 153 Data from all instruments were converted to conservative temperature Θ ($^{\circ}\text{C}$) and
 154 absolute salinity S_A (g kg^{-1}), quality-controlled and cross-calibrated where neces-
 155 sary (see Text S1). Temperature readings from the *Polarstern* thermosalinograph
 156 are excluded here, as they were found to be unreliable (Figure S1). We recommend
 157 not using these data in future analyses.

158 We calculated the mixed layer depth, i.e., the vertical extent of the surface
 159 layer with uniform temperature, salinity, and hence density, as the first depth
 160 where the potential density anomaly σ_0 increases by $\Delta\sigma_0 > 0.04 \text{ kg m}^{-3}$ com-
 161 pared to the surface (4–10 m) mean value (or, 0.06 kg m^{-3} if the increase in
 162 density at the base of the mixed layer was more gradual; see Text S1). We have
 163 omitted giving mixed layer depth estimates in the presence of strong upper (0–
 164 10 m) ocean stratification (i.e., when there is no classical mixed layer, conditions
 165 frequently found during melt season), or when mixed layer depth estimates based
 166 on different density thresholds ($0.04\text{--}0.08 \text{ kg m}^{-3}$) were very variable (i.e., the
 167 base of the mixed layer was not well defined). Surface salinity and temperature
 168 were calculated as the average over 4–10 m depth (to exclude sampling points
 169 within an under-ice meltwater lens in spring for the MSS), and the corresponding
 170 freezing point temperature was calculated based on the TEOS-10 set of equations
 171 (McDougall and Barker, 2011). Additionally, to better identify the surface water
 172 composition and origin, we calculated the surface layer (0–15 m) river water frac-
 173 tion based on an end-member analysis using $\delta^{18}\text{O}$ isotope and salinity measure-
 174 ments (Text S1 and Table S2; Bauch et al., 2011) and colored dissolved organic
 175 matter (CDOM, an indicator for riverine water) fluorescence from ITP94 (before
 176 relocation only; e.g., Granskog et al., 2007; Gonçalves-Araujo et al., 2016; Sted-
 177 mon et al., 2021). We characterized water masses and layers as follows:

- 178 • The surface mixed layer (ML) from the surface to the base of the ML as

- 179 explained above and in Text S1;
- 180 • The halocline layer (HAL) from the base of the ML to $R = \frac{\alpha\Delta\theta}{\beta\Delta S} = 0.05$,
- 181 where α is the thermal expansion and β is the haline contraction coefficient,
- 182 following Bourgain and Gascard (2011);
- 183 • The Atlantic Water thermocline (THERM) from the first depth below the
- 184 halocline where the temperature exceeds 0.8 times the minimum tempera-
- 185 ture in the halocline to the first depth where the temperature exceeds 0.8
- 186 times the maximum temperature of the Atlantic Water layer, as defined in
- 187 Schulz et al. (2021);
- 188 • Arctic Atlantic Water (AAW) as the conservative temperature range $0^\circ\text{C} <$
- 189 $\Theta < 2^\circ\text{C}$ (Korhonen et al., 2013).
- 190 • Atlantic Water (AW) with conservative temperature $\Theta > 2^\circ\text{C}$ (Rudels,
- 191 2012);
- 192 • Upper Polar Deep Water (UPDW) from the first depth when temperatures
- 193 fall below $\Theta = 0^\circ\text{C}$, down to $\sigma_{0.5} = 30.444\text{ kg m}^{-3}$, the potential density
- 194 referenced at 500 m depth (Rudels, 2009);
- 195 • Eurasian Basin Deep Water (EBDW) between $\sigma_{0.5} = 30.444\text{ kg m}^{-3}$ and
- 196 $\sigma_1 = 37.46\text{ kg m}^{-3}$ (Smethie Jr et al., 1988). σ_1 refers to the potential
- 197 density referenced at 1000 m depth;
- 198 • Canadian Basin Deep Water (CBDW) with the same range as EBDW, but
- 199 with $\Theta > -0.6^\circ\text{C}$ and absolute salinity $S_A > 35.083\text{ g kg}^{-1}$ following
- 200 Rudels (2009), with the salinity threshold converted from practical salinity
- 201 of 34.915 in Rudels (2009) at 1500 m depth;
- 202 • Eurasian Basin Bottom Water (EBBW) from $\sigma_1 = 37.46\text{ kg m}^{-3}$ to the sea
- 203 floor (Smethie Jr et al., 1988);
- 204 • In the Yermak Plateau and Fram Strait regions: Arctic Intermediate Water
- 205 (AIW) in the same range as UPDW ($\Theta = 0^\circ\text{C}$ to $\sigma_{0.5} = 30.444\text{ kg m}^{-3}$)
- 206 following Meyer et al. (2017b);
- 207 • In the Yermak Plateau and Fram Strait regions: Nordic Sea Deep Water
- 208 (NSDW) from $\sigma_{0.5} = 30.444\text{ kg m}^{-3}$ to the sea floor (Meyer et al., 2017b).

209 Current velocity profiles (approximately 20–400 m depth) obtained with a

210 75 kHz acoustic Doppler current profiler (ADCP; Baumann et al., 2021) were

211 used to calculate depth-averaged surface layer (14–30 m) and tidal (whole water

212 depth) currents of different frequencies (see Meyer et al., 2017b, and Text S1 for

213 more details on the methodology) and to identify eddies visually. Tidal velocities

214 were then compared to data from the Arctic Ocean Tidal Inverse Model AOTIM5

215 (Erofeeva and Egbert, 2020).

216 Turbulent mixing parameters presented here are based on the dissipation rate
 217 of turbulent kinetic energy ε , measured with the MSS (Schulz et al., 2022b). The
 218 value ε describes how much small (0.1–1 m) scale turbulent kinetic energy (“tur-
 219 bulence”) is present to mix the water column. From ε , we calculated the depth of
 220 the surface active mixing layer, i.e., the depth range where turbulence is elevated
 221 due to friction at the ocean-sea ice interface ($\varepsilon \geq 5 \times 10^{-9} \text{ W kg}^{-1}$). From ε
 222 and the local stratification, we calculated the turbulent diffusivity K_z along each
 223 profile, as described in Bouffard and Boegman (2013). This method takes into ac-
 224 count how K_z scales in different energetic regimes, i.e., in the presence of high
 225 or low turbulence and strong or weak stratification. Spatio-temporal averages in
 226 different regions or over certain vertical layers were obtained using the maxi-
 227 mum likelihood estimator (MLE; Baker and Gibson, 1987) and heat fluxes over
 228 the halocline and thermocline (Section 2) were calculated following Schulz et al.
 229 (2021). In addition, eddy-correlation-based heat fluxes at 3 m depth were mea-
 230 sured with an Autonomous Ocean Flux buoy at a distance of 15–25 km from
 231 *Polarstern* (Stanton et al., 2012; Stanton and Shaw, 2023).

232 We compare four typical Arctic Ocean climatological datasets and two com-
 233 monly used state estimates (i.e., models constrained with observational data to
 234 minimize the misfit to these observations), listed in Table 1, to the MOSAiC data.
 235 These data products cover different time periods, contain different types of data
 236 from various sources and are produced using distinct methods and interpolation
 237 procedures (see Text S1 for details).

Table 1. Climatologies and state estimates (*italics*) of temperature and salinity used for comparison with the MOSAiC observations (Section 7).

Dataset	Reference	Vertical layers	Temporal coverage
PHC3	Steele et al. (2001)	24	1948–1997
WOA18	Locarnini et al. (2018); Zweng et al. (2018)	57	1955–2017
MIMOC	Schmidtko et al. (2013)	81	1970–2011
WOA23	Boyer et al. (2018)	57	1991–2020
<i>ASTE</i>	Nguyen et al. (2021)	50	2002–2017
<i>ECCOv4</i>	Forget et al. (2015)	50	1992–2015

238 3. Geography along the drift track

239 The Arctic Ocean is a semi-enclosed basin, connected to the Atlantic Ocean via
 240 Fram Strait between Svalbard and Greenland and the Barents Sea and to the Pa-

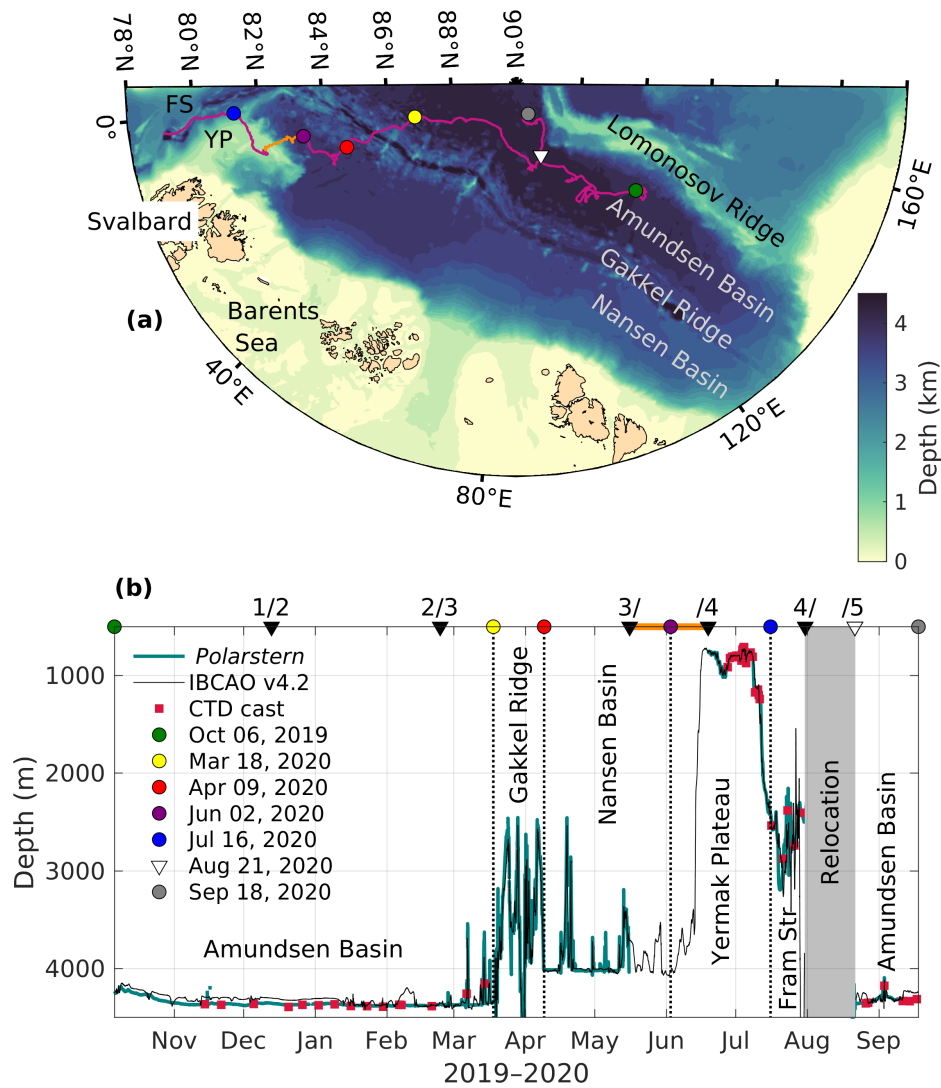


Figure 1. Bathymetry along the drift track.

(a) Bathymetric map of the Arctic Ocean with drift track (violet from *Polarstern*, orange from positioning buoy "CO1" between Legs 3 and 4) indicated; (b) bathymetry along the drift track from the *Polarstern* echosounder (teal), International Bathymetric Chart of the Arctic Ocean (IBCAO v4.2) data set (black) and the deep conductivity, temperature, depth (CTD) casts (red squares). For better orientation, landmarks of the drift and the start and end of the individual legs are indicated with colored dots and triangles in both panels. The orange line in (b) indicates the time period when the floe was left uncrewed.

241 cific via the Bering Strait between Russia and Alaska. Surrounded by wide shelf
242 seas, the deep Arctic basin is separated by the Lomonosov Ridge, which reaches
243 from the Siberian shelf to the Canadian shelf, into the Amerasian and Eurasian
244 basins. The Eurasian Basin is further divided into the Amundsen Basin and the
245 Nansen Basin by the Gakkel Ridge (Figure 1a). The shallow Yermak Plateau ex-
246 tends northwards from the continental shelf on which the Svalbard archipelago is
247 located, with the Nansen Basin on its eastern side and Fram Strait on its western
248 side. These geographic divides have a large impact on Arctic Ocean circulation
249 patterns and hence on the water column structure in the different regions. When
250 interpreting the results from a drift campaign such as MOSAiC, regional gradients
251 have to be taken into account.

252 The MOSAiC drift started in October 2019 in the 4400 m deep Amundsen
253 Basin (green dot in Figure 1) and progressed parallel to the Gakkel Ridge within
254 the basin over virtually flat bottom topography for around 5 months. The drift
255 then crossed the rough topography of the Gakkel Ridge over a 3-week time period
256 between March 18 and April 9, 2020 (yellow to red dot in Figure 1), and crossed
257 the Nansen Basin. At the beginning of June, the drift reached the shallow Yermak
258 Plateau (local depth approximately 800 m; purple dot in Figure 1) northwest of
259 Svalbard. After crossing the plateau from east to west, the floe entered the deeper
260 waters and complex topography of Fram Strait on July 16 (blue dot in Figure 1)
261 and drifted south, until the floe eventually broke up in the marginal ice zone.
262 After a relocation closer to the North Pole, in the vicinity of the previous drift
263 track (white triangle in Figure 1), measurements were resumed on a second floe
264 in the Amundsen Basin. This time, the drift was directed northwards, parallel to
265 the Lomonosov Ridge, until the expedition ended on September 20, 2020.

266 Compared to the water depth measurements from MOSAiC, we found that the
267 bathymetric data from IBCAO v4.2 perform well in the basins and for the Gakkel
268 Ridge and Yermak Plateau region, but agree less well with the highly variable
269 bottom depth in Fram Strait. In the following, we use the bathymetric data from
270 IBCAO and any basin averages (e.g., of temperature and salinity profiles) refer to
271 averages over the regions indicated above and in Figure 1b, with a discrimination
272 between conditions in the Amundsen Basin during winter (first part of the drift)
273 and during summer (last part of the drift).

274 4. Water column structure and variability

275 In the following sections, we provide a short general overview of the water masses
276 of the Eurasian Arctic Ocean and their formation and characteristics (Section 4.1).

277 We then elaborate on the observed variability of the near-surface waters (Sec-
278 tion 4.2), the Atlantic Water layer (4.3) and the deep water masses (Section 4.4)
279 during the MOSAiC drift.

280 *4.1. Water masses in the Arctic Ocean*

281 Large amounts of terrestrial freshwater (and other material) enter the Arctic Ocean
282 from Siberia and are advected towards Fram Strait together with sea ice formed
283 on the Siberian shelves transported via the Transpolar Drift (e.g., Mysak, 2001;
284 Karcher et al., 2012; Rudels, 2012; Charette et al., 2020). Both the transport of
285 freshwater and sea ice across the Arctic Ocean are often referred to as the "Trans-
286 polar Drift". While both transport patterns are qualitatively similar, the exact trans-
287 port pathway and the velocities of sea ice and river water-rich surface water differ
288 (see Section 5). In this study, Transpolar Drift refers to the transport of relatively
289 fresh, river water-rich surface water from Siberian regions towards Fram Strait
290 unless specified otherwise.

291 The surface waters within the Transpolar Drift are characterized by high
292 concentrations of dissolved organic carbon (DOC) and various lithogenic ele-
293 ments and may carry organisms originating from the coastal and shelf zones
294 (Krumpfen et al., 2019; Charette et al., 2020). Paffrath et al. (2021) showed, based
295 on lithogenic provenance tracers, that most of the freshwater encountered in the
296 Eurasian Arctic Ocean is derived from the Lena, Yenisei and Ob rivers, whose
297 contributions do not fully mix and form distinct freshwater domains within the
298 Transpolar Drift. The high nutrient loads in these terrestrial waters is partially uti-
299 lized on the wide Siberian shelves (Laukert et al., 2022), and their role for primary
300 production at the pan-Arctic scale is still not entirely clear (Fouest et al., 2013; Ter-
301 haar et al., 2021; Gibson et al., 2022). Mixed with ambient waters, this land-runoff
302 forms a relatively fresh surface layer uniform in temperature and salinity: the po-
303 lar mixed layer (ML; gray in Figure 2c of the MOSAiC data). This surface layer
304 is bound by a pycnocline, i.e., a sharp increase in density, primarily set by salinity
305 here, over a few meters, which we refer to as the base of the surface mixed layer.
306 Below, salinity increases further, but more gradually, i.e., over tens of meters, with
307 temperatures at or close to the freezing point. This layer is called the Arctic halo-
308 cline (teal in Figure 2c, Schauer et al., 1997; Rudels, 2012). In temperature and
309 salinity space (i.e., TS-diagrams), the halocline appears as an increase in salinity
310 close to the freezing point line (as in Figure 3a). Due to its strong stratification,
311 the halocline suppresses the vertical exchange between the surface layer and un-
312 derlying waters (Schulz et al., 2023a) and prevents both heat and nutrients from

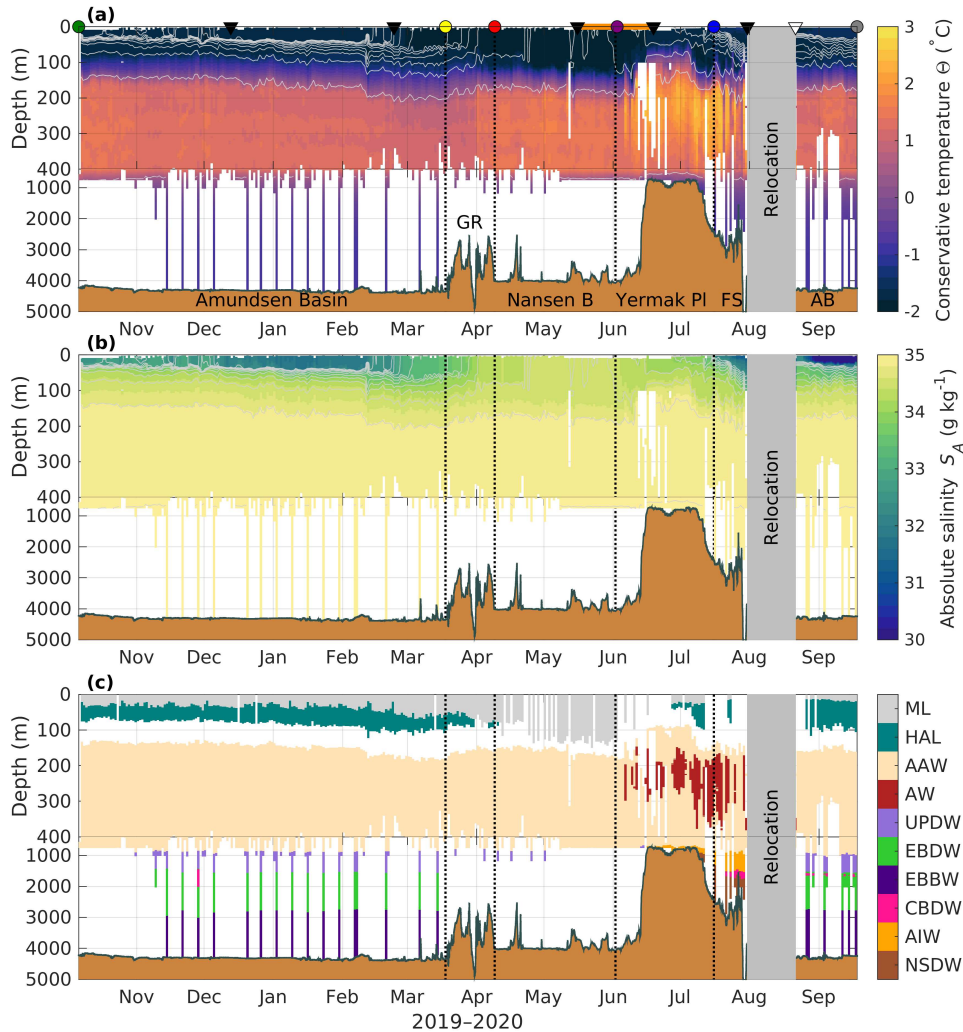


Figure 2. Water mass distribution along the drift.

(a) Conservative temperature ($^{\circ}\text{C}$), (b) absolute salinity (g kg^{-1}) and (c) water mass distribution along the drift, based on the composite dataset presented in this study. In (a–c), topographic regions are shown (in brown), including the Amundsen Basin (AB), Gakkel Ridge (GR), Nansen Basin (B), Yermak Plateau (PI) and Fram Strait (FS); the white regions have no data coverage. Gray lines in (a) and (b) indicate isopycnals with a spacing of 0.2 kg m^{-3} . The color bar in (c) indicates the mixed layer (ML), halocline (HAL), Arctic Atlantic Water (AAW), Atlantic Water (AW), Upper Polar Deep Water (UPDW), Eurasian Basin Deep Water (EBDW), Eurasian Basin Bottom Water (EBBW), Canadian Basin Deep Water (CBDW), Arctic Intermediate Water (AIW) and Nordic Sea Deep Water (NSDW). Data gaps in June are caused by ice-tethered profiler (ITP) data not covering the whole water column. Note that the y-axis is nonlinear, zoomed in the upper 400 m. In (a), triangles indicate the start and end of the legs; dots and vertical dotted lines, the geographical markers; and the orange line, the uncrewed period of the drift as in Figure 1b.

313 the Atlantic Water layer to reach the surface. In addition, the strong stratification
314 also decouples the speed and even direction of lateral advection in the surface
315 layer and halocline, which may all contribute to a heterogeneous distribution of
316 tracers as well as microorganisms in these layers, despite both being located in the
317 potentially sun-lit upper ocean.

318 Relatively warm and saline water from the Atlantic enters the Arctic Ocean
319 through eastern Fram Strait and the shallow Barents Sea, carrying high nutri-
320 ent concentrations (Torres-Valdés et al., 2013) and organisms of Atlantic origin
321 (Snoeijs-Leijonmalm et al., 2022). This water circulates counterclockwise along
322 the Arctic continental slopes (Schauer et al., 1997; Rudels, 2012) and is modified
323 on its pathway by heat loss to the atmosphere when it resides close to the surface
324 in the Barents Sea (Smedsrud et al., 2013; Meyer et al., 2017a) and subsequently
325 by mixing with colder water masses (Lenn et al., 2009; Rippeth et al., 2015). This
326 modification appears as a temperature decrease and a progressively deeper po-
327 sition of the warm and saline Atlantic Water within the water column along its
328 advective pathway (e.g., Schulz et al., 2021). When Atlantic Water temperatures
329 are below 2°C, we refer to it as modified, or Arctic Atlantic Water (AAW; beige
330 in Figure 2c). In TS-diagrams, this layer is visible as a temperature peak, i.e., an
331 increase and decrease of temperature over a narrow salinity range (Figure 3a). The
332 distribution and modification of Atlantic Water can also be inferred from provenance
333 tracers (e.g., Bauch et al., 2016; Laukert et al., 2017, 2019).

334 The identification of deep waters below the Atlantic Water layer is less
335 straightforward, as changes in temperature and salinity at these depths can be
336 close to the instrument precision (as in the MOSAiC data, red box in Figure 3).
337 Moreover, historical definitions for these deep waters might not hold anymore, as
338 the properties of the water masses involved in their formation have been chang-
339 ing due to ongoing global warming (Somavilla et al., 2013; von Appen et al.,
340 2015; Karam et al., 2024). Here, we use a set of historical definitions that dif-
341 fer between the central basins and the regions of Yermak Plateau and Fram Strait
342 (see Section 2), but we advise treating these results with caution. In the central
343 Eurasian Arctic Ocean (Amundsen and Nansen Basins), Upper Polar Deep Water
344 (UPDW; lilac in Figure 2c) resides below the Atlantic Water layer. UPDW is a het-
345 erogeneous water mass formed as a mixture of intermediate waters, flowing into
346 the Arctic Ocean through Fram Strait, and Atlantic Water that has been strongly
347 cooled during winter in the Barents Sea, as well as saline and dense plumes formed
348 on the shelves by brine rejection during sea ice formation (e.g., Rudels, 2009). In
349 the TS-diagram, this water mass is a mostly straight line with increasing salin-
350 ity and decreasing temperature (Figure 3b). Below the UPDW, the primary water

351 mass is Eurasian Basin Deep Water (EBDW; green in Figure 2c), with occasional
352 intrusions of relatively warm and saline Canada Basin Deep Water (CBDW; pink
353 in Figure 2c). EBDW is characterized by nearly constant temperature and is the
354 result of the interaction between inflowing deep waters through Fram Strait and
355 dense plumes from the shelves (e.g., Smethie Jr et al., 1988). CBDW enters the
356 Eurasian Basin across the Lomonosov Ridge and proceeds as a narrow boundary
357 current, but is episodically transported into the interior basin by eddies (Karam
358 et al., 2023). The water mass close to the seafloor is called Eurasian Basin Bottom
359 Water (EBBW; dark purple in Figure 2c); its properties are impacted notably by
360 dense overflows and geothermal heating (e.g., Smethie Jr et al., 1988). In Fram
361 Strait, there is Arctic Intermediate Water (AIW; orange in Figure 2c) instead of
362 UPDW below the Atlantic Water layer and Norwegian Sea Deep Water (NSDW;
363 brown in Figure 2c) closer to the sea floor. AIW is characterized by nearly constant
364 salinity and decreasing temperatures with depth and is typically enriched in
365 oxygen, as it is formed through open ocean convection in the Nordic Seas (e.g.,
366 Meyer et al., 2017b). NSDW used to be seen as a cold, fresh and very dense water
367 mass but has warmed rapidly since the cessation of Nordic Seas deep convection,
368 as it is no longer replenished. It now closely resembles EBDW (von Appen et al.,
369 2015; Karam et al., 2023). All the deep water masses are different mixtures be-
370 tween water of Atlantic origin and waters entrained by deep convection (NSDW)
371 or dense water overflows (all Eurasian basins deep waters) and therefore have
372 different tracer properties, especially oxygen (Karam et al., 2023) and transient
373 tracers (Heuzé et al., 2023a).

374 4.2. *Surface and subsurface layer properties along the MOSAiC* 375 *drift*

376 The Amundsen Basin of early winter 2019–2020 was characterized by a well-
377 defined surface mixed layer close to the freezing point down to around 30 m depth
378 and a stable halocline below (Figure 4a,d). Intermediate surface salinities around
379 33 g kg^{-1} combined with low CDOM concentrations (Figure 4b,c) suggest that the
380 contribution of river water was relatively small here. This small contribution could
381 be related to different freshwater sources and their respective advective pathways,
382 as the distribution of neodymium isotopes indicates alternating freshwater do-
383 mains in this region reflecting variable contributions from the Yenisei, Ob and
384 Lena rivers (G Laukert, unpublished). Sea ice meltwater from the preceding melt
385 season may have also contributed to a fresher surface layer in this region (com-
386 pared to the water below) and diluted the river-borne compounds. This dilution

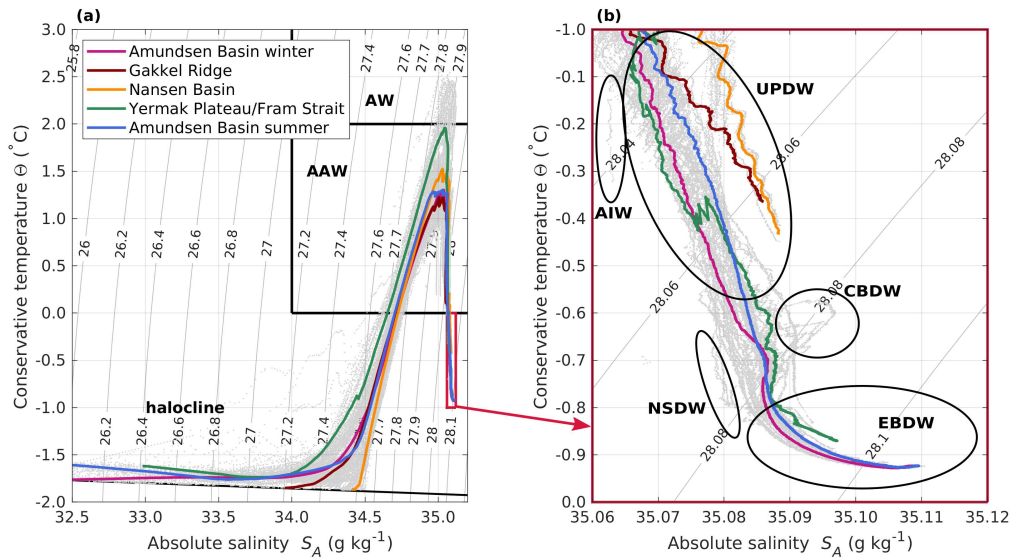


Figure 3. Temperature-salinity diagrams.

Absolute salinity against conservative temperature for (a) the full depth range (for the basin averages, the upper 5 m are not shown); and (b) enlargement of the deep water masses. Gray lines indicate daily profiles and colored lines refer to basin averages as indicated. The black line in (a) indicates the salinity-dependent freezing point temperature, and black rectangles indicate Atlantic Water (AW) and Arctic Atlantic Water (AAW). The small pink rectangle in (a) corresponds to the range displayed in (b). In (b), circles indicate the approximate range of Upper Polar Deep Water (UPDW), Eurasian Basin Deep Water (EBDW), Canadian Basin Deep Water (CBDW), Arctic Intermediate Water (AIW) and Nordic Sea Deep Water (NSDW).

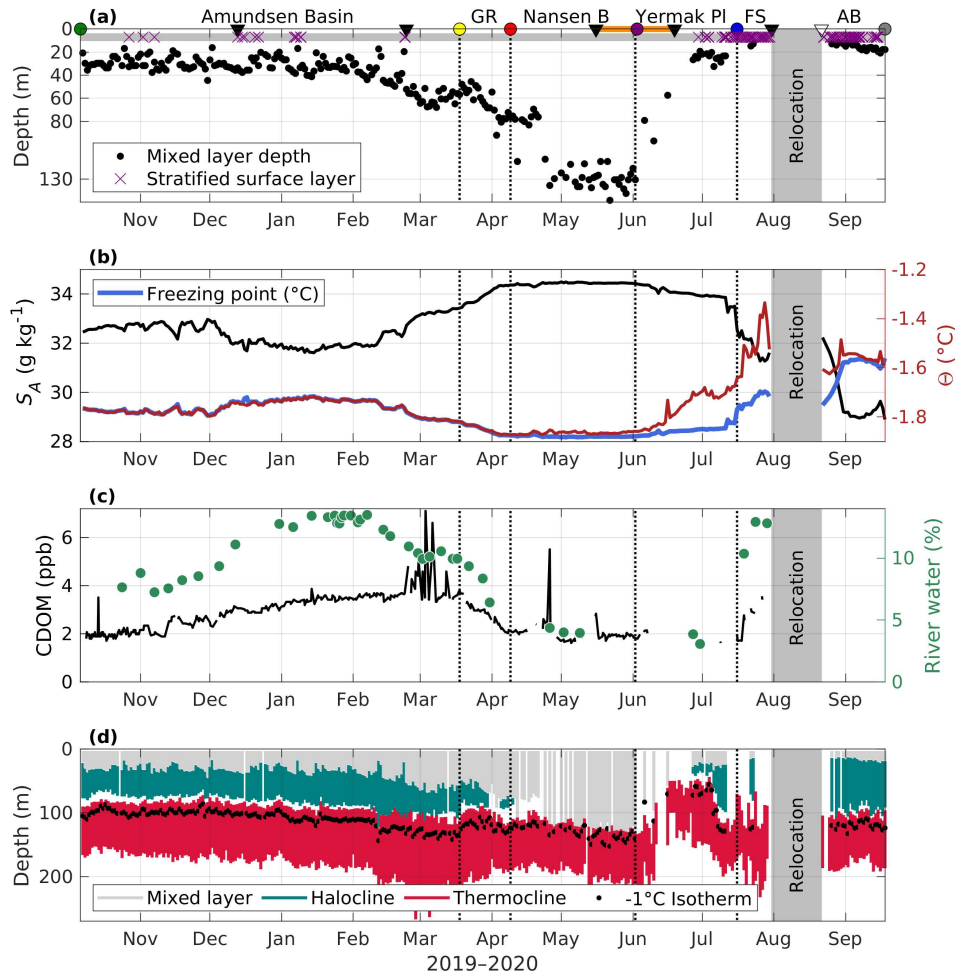


Figure 4. Ocean surface layer properties along the drift.

(a) Surface mixed layer depth (m, black dots; stratified surface layers are indicated with purple crosses), (b) surface absolute salinity (g kg^{-1} , black line), conservative temperature Θ ($^{\circ}\text{C}$, red line) and freezing point temperature ($^{\circ}\text{C}$, blue line), (c) colored dissolved organic matter (CDOM; ppb, black line) and river water fraction (%), green dots) and (d) mixed layer (gray), halocline (teal) and thermocline (red) extent and position of the -1°C isotherm (black dots) along the drift. In (a), triangles indicate the start and end of the legs; dots, vertical dotted lines and annotations, the geographical markers including Amundsen Basin (AB), Gakkel Ridge (GR), Nansen Basin (B), Yermak Plateau (PI) and Fram Strait (FS). The orange line indicates the uncrewed period of the drift as in Figure 1b.

387 effect could explain the rather low dissolved organic carbon (DOC) concentra-
388 tions at the very start of the drift (Kong, 2022). At the beginning of December,
389 a decrease in salinity and an increase in both CDOM and river water fraction
390 (derived from $\delta^{18}\text{O}$; see Section 2, Text S1) to over 13% indicate that the floe
391 had entered the river water-rich part of the Transpolar Drift. Somewhat surpris-
392 ingly, the position of the maximum river water fraction does not coincide with
393 the highest concentrations of CDOM, which appear only when surface salinity in-
394 creases again and the surface layer started to deepen in March (Figure 4a–c). This
395 disjunct could be related to different freshwater sources and their respective ad-
396 vective pathways, as the distribution of neodymium isotopes indicates alternating
397 freshwater domains in this region either reflecting increased contributions from
398 the Yenisei and Ob rivers or the Lena River (G Laukert, unpublished). A similar
399 but spatially shifted distribution has already been described based on summer data
400 from 2015, suggesting a strong spatio-temporal variability of the surface waters
401 in the Eurasian Arctic Ocean (Paffrath et al., 2021).

402 As it approached the Gakkel Ridge, the floe left the heavily river-water-
403 influenced part of the Transpolar Drift and surface salinity increased to a max-
404 imum of 34.3 g kg^{-1} . River water fraction and CDOM concentrations decreased
405 during the passage of the ridge (Figure 4c). These decreases were also coinci-
406 dent with a decrease of DOC concentrations in the surface layer (Kong, 2022).
407 On the Nansen Basin side of the Gakkel Ridge, the surface mixed layer deepened
408 to around 80 m. At the end of April, the surface stratification, i.e., the halocline,
409 disappeared completely and density only increased at a depth of approximately
410 130 m. These conditions have previously been described as "deep ventilation"
411 (Polyakov et al., 2017), referring to a mixed layer that is not bounded by the
412 halocline but reaches down to the warm Atlantic Water layer. This enhanced con-
413 nectivity between the surface and Atlantic layer, compared to the situation in the
414 Amundsen Basin, is also evident from provenance tracer distributions suggest-
415 ing enhanced Atlantic Water admixture to the surface (G Laukert, unpublished)
416 and might promote the transport of deep oceanic heat towards the sea ice (see
417 Section 6), thereby slowing basal growth (Lei et al., 2022), and increase verti-
418 cal nutrient supply to the surface layer (Randelhoff et al., 2020). The enhanced
419 vertical exchange might also facilitate the transport of organisms advected in the
420 Atlantic Water layer closer to the surface. Deep ventilation, along with relatively
421 constant surface salinity, low river water fraction and CDOM concentrations, per-
422 sisted throughout the Nansen Basin until the drift reached the Yermak Plateau in
423 June (Figure 4).

424 Above Yermak Plateau, from the end of May onwards, surface layer temper-

425 atures increased successively with ongoing solar warming and deviated more and
426 more from the freezing point (Figure 4b). River water fraction and CDOM re-
427 mained at the same low levels as encountered in the Nansen Basin, but a slightly
428 lower surface salinity allowed for the presence of a halocline. The Atlantic Water
429 layer on the eastern side and above the plateau was much shallower (see Sec-
430 tion 4.3), restricting the vertical extent of the halocline (Figure 4d). Sea ice melt,
431 starting in late May to early June (Lei et al., 2022; Webster et al., 2022), and
432 surface warming created vertical density differences, i.e., stratification, within the
433 near-surface layer. Turbulent mixing in the upper ocean (see Section 6 for details)
434 did not penetrate deeper than 30 m and usually was not strong enough to destroy
435 the near-surface stratification established by meltwater input and warming. Hence,
436 especially later in the season, we often observed no classical surface mixed layer
437 (purple crosses in Figure 4a) and, even in the uppermost layer, vertical gradients in
438 any tracer concentration, e.g., nutrients, or organism distribution, can be expected.

439 When leaving the Yermak Plateau on July 16, we observed another regime
440 shift in the surface layer: Surface salinity abruptly decreased, while river water
441 fraction and CDOM concentrations, which had remained low since entering the
442 Nansen Basin, increased. This change is accompanied by a trend toward less ra-
443 diogenic neodymium isotopic compositions (G Laukert, unpublished), suggesting
444 increased admixture of Lena River water and supporting cross-Arctic transport
445 of Siberian freshwater. In Fram Strait, we also observed a subsurface increase of
446 CDOM (data not shown), indicative of the "edge" of the East Greenland Current
447 (which is an extension of the Transpolar Drift of relatively fresh water of Siberian
448 origin). Such a transition from one oceanic (surface) regime to another is often
449 accompanied by sudden changes in biogeochemical water properties (e.g., nutri-
450 ent relationships) and potentially also the ecological community structure (e.g.,
451 Tippenhauer et al., 2021). The surface temperature anomaly relative to freezing
452 point further increased, to a maximum of 0.4°C shortly before the floe broke up.

453 After relocating north at the end of August, back into the Amundsen Basin,
454 we observed the freshest surface waters (see also Rabe et al., 2022) and a sta-
455 ble halocline similar to the first phase of the drift. There are no sensor-based
456 CDOM measurements after the relocation, but the highest CDOM absorption and
457 DOC concentrations in surface waters during MOSAiC were found here (Kong,
458 2022). Moreover, the highest river water fractions based on oxygen isotopes and
459 the least radiogenic neodymium isotope signatures were determined, in line with
460 the strongest Lena River contributions during the entire MOSAiC campaign (G
461 Laukert, unpublished). The similarity of neodymium isotope signatures between
462 this freshwater domain and that in the western Fram Strait may suggest continuous

463 freshwater transport along the Transpolar Drift. However, enhanced freshwater
464 export from the Siberian shelf exhibits a strong seasonality linked to the variable
465 shelf hydrography (Janout et al., 2020), which may be preserved along the Trans-
466 polar Drift. The uppermost layer was often stratified due to sea ice melt and solar
467 warming. Whenever a well-defined surface layer existed, it was about 20 m deep,
468 slightly shallower than during the first part of the drift. Surface temperatures were
469 still above freezing when sampling resumed, but approached freezing point at the
470 beginning of September.

471 When sampling was resumed after the floe had been left uncrewed in July, we
472 observed an approximately 1 m thick, low-salinity (S_A from close to 0 to about
473 10 g kg^{-1}) under-ice meltwater layer, visible in salinity profiles (Schulz et al.,
474 2022b). At the interface between the fresher meltwater layer and the underlying
475 colder seawater, thin layers of ice formed, so-called false bottoms (Smith et al.,
476 2022; Salganik et al., 2023a). Low salinity meltwater layers in leads remained
477 present until strong winds caused enhanced mixing during the period September
478 5–9 (Smith et al., 2023; Nomura et al., 2023). The presence of meltwater resulted
479 in a very strong stratification in the uppermost meters, up to two orders of mag-
480 nitude stronger compared to the halocline. Measurements with an uprising turbu-
481 lence profiler also show drastically reduced turbulent mixing in the near-surface
482 layer when meltwater layers were present (Fer et al., 2022). Details on the dy-
483 namics and implications of meltwater layers can be found in Smith et al. (2022);
484 Nomura et al. (2023); Salganik et al. (2023a); Smith et al. (2023).

485 4.3. *Atlantic Water layer along the MOSAiC drift*

486 Modified Arctic Atlantic Water (AAW) was present throughout the MOSAiC drift.
487 In the Amundsen Basin, the upper limit of the AAW layer were situated at approx-
488 imately 150 m depth. After passing the Gakkel Ridge into the Nansen Basin, the
489 AAW was warmer and situated deeper in the water column (Figure 2a). Relatively
490 unmodified Atlantic Water (AW), coming straight from the Atlantic and being
491 characterized by a core temperature above 2°C , was only present above Yermak
492 Plateau (Figure 2c), where warm waters also resided about 100 m closer to the sur-
493 face (Figure 4d), and in Fram Strait. Here, we use the term Atlantic Water (layer)
494 to refer to both AW and AAW.

495 The "older" the Atlantic Water layer, i.e., the longer it has been out of contact
496 with the surface and traveled in the Arctic while being mixed with colder wa-
497 ters, the deeper and colder its core (Rudels, 2015). Hence, we observed a strong
498 correlation ($R^2 = 0.67$, not shown) between the core depth and the core tempera-

499 ture. Along the drift in 2019–2020, the Atlantic Water core was mostly located at
500 around 300 m depth, with a temperature around 1.2°C. Above Yermak Plateau and
501 in Fram Strait, the core was approximately 1°C warmer (and 0.1 kg m⁻³ lighter)
502 and 100 m shallower, but subject to strong variability. In this region, the impact
503 of the shallow and "young" Atlantic Water on, e.g., nutrient supply or organism
504 composition might be more pronounced compared to the situation in the deep
505 basins.

506 As Atlantic Water can take different paths within the Arctic Ocean, e.g., en-
507 tering via Fram Strait or through the Barents Sea, or recirculating into the deep
508 basins from different positions along the continental slope (Rudels, 2012, 2015),
509 different branches of Atlantic Water, with slightly different temperature and salin-
510 ity signatures, can often be found at the same position, stacked on top of each other
511 (Rudels and Hainbucher, 2020). These "interleaving" layers can be identified as
512 z-shapes near the Atlantic Water temperature maximum in the TS-diagrams (Fig-
513 ure 3a) and as inversion layers and local temperature minima in the temperature
514 profiles. In the Amundsen and Nansen Basin, interleaving involved mainly the
515 Barents Sea and the Fram Strait branches of Atlantic Water. In the more dynamic
516 Fram Strait region, we found strong interleaving, with several sources of Atlantic
517 Water, which might differ in their respective biogeochemical signature that cause
518 vertical gradients in, e.g., nutrient concentration.

519 At the upper bound of the Atlantic Water layer, both temperature and salin-
520 ity increase with depth. In quiescent conditions, i.e., when turbulent mixing is
521 negligible and molecular diffusion is the dominant mixing process, temperature
522 gradients diffuse faster than gradients in salinity. This difference in thermal and
523 haline diffusion coefficients creates step-like structures, so-called thermohaline
524 or double-diffusive staircases, typical for the Arctic Ocean (Shibley et al., 2017).
525 These structures can persist for years and over 100 km of horizontal distance, and
526 individual layers can be up to several tens of meters thick (e.g., Lenn et al., 2009;
527 Guthrie et al., 2017). Along the MOSAiC drift, we frequently, but not always,
528 observed thermohaline staircases in the quiescent Amundsen Basin, in line with
529 findings from high resolution observations from drifting stations in the same area,
530 that show 1–3 m thick thermohaline staircase layers in the 200–260 m depth range
531 (Sirevaag and Fer, 2012). Outside of the Amundsen Basin, we sometimes ob-
532 served structures that might be remnants of thermohaline staircases in the vertical
533 profiles (not shown), but their characteristic sharp interfaces were absent. These
534 differences point towards a lower connectivity between the surface and deeper
535 ocean in the Amundsen Basin, compared to the other parts of the drift.

536 4.4. *Deep water along the MOSAiC drift*

537 The deep water masses during the MOSAiC drift have been described in detail in
538 Karam et al. (2023) and Rabe et al. (2022); here, we provide only a brief sum-
539 mary. Despite the uncertainties associated with the identification of deep water
540 masses (sensor accuracy, changes in end member properties; see Section 4.1), we
541 observed a somewhat consistent distribution of deep waters across the Eurasian
542 basin during MOSAiC. In the Nansen and Amundsen Basin, UPDW was ob-
543 served right under the Atlantic layer down to approximately 1500 m. Below the
544 UPDW, primarily EBDW is found until the sill depth of Fram Strait (approx-
545 imately 2500 m), with occasional intrusions of relatively warm and saline CBDW
546 as a salinity maximum between 1700–2000 m depth (Karam et al., 2023). Below
547 the sill depth of Fram Strait, the temperature increased slightly as we encountered
548 the last deep water mass, EBBW, until the seafloor. Deep waters directly above
549 the Gakkel Ridge and their unique hydrothermal-vent-influenced ecosystem were
550 not sampled during MOSAiC.

551 The deeper waters above the Yermak Plateau and in Fram Strait consisted
552 of UPDW, alternating with likely AIW. Below UPDW/AIW, we again observed
553 CBDW in Fram Strait, as a salinity maximum at roughly 2000 m depth. Close to
554 the bottom in Fram Strait, we found a mixture of NSDW and EBDW. Again, we
555 note that identifying water masses in Fram Strait solely based on their temperature
556 and salinity signature as done in this study is associated with large uncertainties,
557 primarily due to the warming and increased salinity of waters south of Fram Strait
558 over the past decades. Hence, traditional water mass classifications (Marnela et al.,
559 2016) do not necessarily hold for the deep waters anymore (Somavilla et al., 2013;
560 von Appen et al., 2015). Other tracers, such as CFC, SF₆, or dissolved oxygen, are
561 needed to accurately determine the origin of deep water masses, which is beyond
562 our scope but addressed in Karam et al. (2023) and Heuzé et al. (2023a).

563 5. Current velocities, tides and eddies

564 In both central basins, current velocities below the surface mixed layer were small,
565 on the order of 0.01 m s⁻¹. Within the surface mixed layer, current velocities were
566 intensified and correlated with the sea ice drift speed ($R^2 = 0.9$; data not shown).
567 The magnitude of the ocean surface current (14–30 m vertical average), however,
568 was much smaller, on average 16% of the floe drift speed (Figure 5a), meaning that
569 the ice moves around six times faster than the upper ocean. This difference illus-
570 trates that, while both sea ice and fresh, riverine water are transported from their
571 region of origin in Siberia across the Arctic towards Fram Strait, their transport

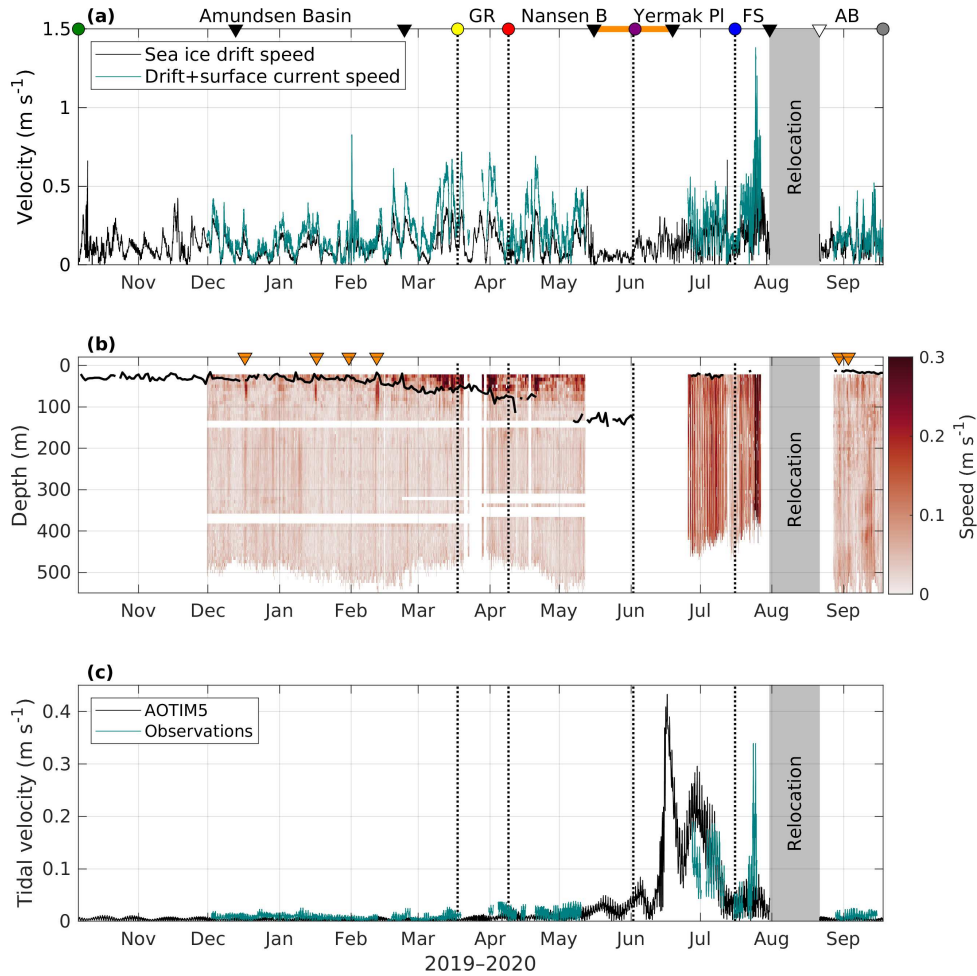


Figure 5. Current velocities along the drift.

(a) Sea ice drift (black, m s^{-1}) and combined drift and averaged current velocity in the upper 14–30 m relative to the floe (teal, m s^{-1}), (b) current speed (m s^{-1}) relative to the sea floor and (c) tidal velocities (m s^{-1}) from observations (teal) and the Arctic Ocean Tidal Inverse Model AOTIM5 (black) along the drift. In (a), triangles indicate the start and end of the legs, dots, vertical dotted lines and annotations the geographical markers including Amundsen Basin (AB), Gakkel Ridge (GR), Nansen Basin (B), Yermak Plateau (PI) and Fram Strait (FS). The orange line indicates the uncrewed period of the drift as in Figure 1b. In (b), orange triangles indicate near-surface eddies, the black line indicates the depth of the surface mixed layer.

572 timescales and exact pathways differ. Sea ice within the Transpolar Drift typically
 573 traverses the Arctic Ocean within 1–3 years (Charette et al., 2020; Steele et al.,
 574 2004), while the transport timescale for freshwater might be rather on the order of
 575 a decade. In addition, the pathway of the Transpolar Drift is strongly influenced
 576 by daily to decadal variability in wind conditions (Mysak, 2001), yielding that
 577 liquid and solid freshwater of similar origin in space and time might take very
 578 different routes through the Arctic Ocean. The difference in sea ice drift and sur-
 579 face ocean current speed also underlines that, while sampling the same sea ice, the
 580 water below the ice quickly changes throughout the drift and oceanic data cannot
 581 be treated as a simple time series. Furthermore, as the surface mixed layer tends
 582 to move faster than the ocean below, any time series recorded above and below
 583 the surface mixed layer base might develop independently of each other.

584 The region around the Yermak Plateau and especially in Fram Strait, is more
 585 energetic. Absolute current velocities were much higher (up to 0.4 m s^{-1}) and
 586 more variable, and surface currents correlated less with sea ice drift. Here, tides
 587 play a greater role, with a dominance of diurnal frequencies above the Yermak
 588 Plateau and semi-diurnal frequencies in Fram Strait (data not shown; see Fer et al.,
 589 2015, for details on tides in the region). In combination with the more variable
 590 water column structure in this region (see Section 4), we expect more variability
 591 on short, daily to sub-daily, timescales, e.g., in surface nutrient supply or species
 592 composition. Assumptions of lateral homogeneity, i.e., negligible spatial gradi-
 593 ents, which are to some degree justified in the respective deep basins, no longer
 594 hold in the dynamic regime of the Yermak Plateau and Fram Strait.

Table 2. Clearly identifiable upper ocean eddies along the drift.

Start	End	D ^a (m)	Δh ^b (m)	Type
17.12.19 01:00	18.12.19 11:00	38	40	Anticyclonic
16.01.20 07:00	17.01.20 10:00	38	48	Anticyclonic
31.01.20 08:00	02.02.20 07:00	22	56	Anticyclonic
11.02.20 14:00	13.02.20 12:00	22	80	Anticyclonic
29.08.20 17:00	30.08.20 17:00	38	40	Cyclonic
03.09.20 23:00	03.09.20 10:00	30	64	Anticyclonic

^a First depth where the eddy was detected.

^b Vertical eddy thickness.

595 Six upper ocean eddies were identified in the halocline in the Amundsen and
 596 Nansen Basin, listed in Table 2 and indicated in Figure 5b. Five of these eddies

597 rotated anticyclonically (clockwise) and only one cyclonically, in line with the
598 previously reported prevalence of anticyclonic eddies in the Arctic Ocean (Zhao
599 et al., 2014; von Appen et al., 2022). The timing of these eddies does not coincide
600 with the presence of storms or strong winds, indicating that the eddies had not
601 been formed locally, but might rather be advected and originate from topographic
602 features (Zhao et al., 2014) or barotropic and baroclinic instabilities (von Ap-
603 pen et al., 2022). Eddies can transport water masses with distinct biogeochemical
604 signatures over large distances, and their associated higher current velocities can
605 increase local vertical mixing (Son et al., 2022). Both processes can enhance the
606 nutrient supply to the photic zone, making eddies potential biological hotspots.
607 A presumably high fraction of nutrients supplied by eddy activity in the Arctic
608 winter would not be consumed, but would instead (locally) increase the nutrient
609 inventory for the next productive season. In addition, anticyclonic eddies are as-
610 sociated with a shoaling of the mixed layer base, which was most pronounced for
611 the eddies in January and February when the mixed layer depth decreased by 10–
612 20 m. However, a similar variability in mixed layer depth is also observed during
613 times when eddies were absent. In the Yermak Plateau/Fram Strait regions, eddy
614 activity is obscured by the strong tides; hence no eddies were identified there.

615 On November 9, 14 and 28 (2019), we also observed a large anticyclonic eddy
616 at greater depth in the middle of the Amundsen Basin, indicated by sloping isopy-
617 cnals above and below the eddy, with relatively dense waters above the eddy and
618 light waters below, relative to the adjacent water column (data not shown). This
619 eddy carried a warm and saline CBDW intrusion and extended over approximately
620 1200–2400 m depth (Karam et al., 2023).

621 6. Turbulence and vertical transport

622 6.1. *Surface mixing*

623 In contrast to the surface *mixed* layer depth, which describes the depth to which
624 the surface layer is uniform in temperature and salinity (see Section 4.2), the
625 *mixing* layer depth describes how deep active turbulent mixing, which is created
626 by friction at the ice-ocean interface, or by wind and waves in the marginal ice
627 zone or open water conditions, penetrates into the water column. While active
628 mixing creates the mixed layer by homogenizing the water column, the mixed
629 layer will persist even after the active mixing has decayed. This persistence is be-
630 cause, even though the small-scale turbulent motion causing the mixing will dissi-
631 pate within hours or days, the re-establishment of gradients near the surface, i.e.,
632 re-stratification, often takes much longer, especially in the absence of restoring

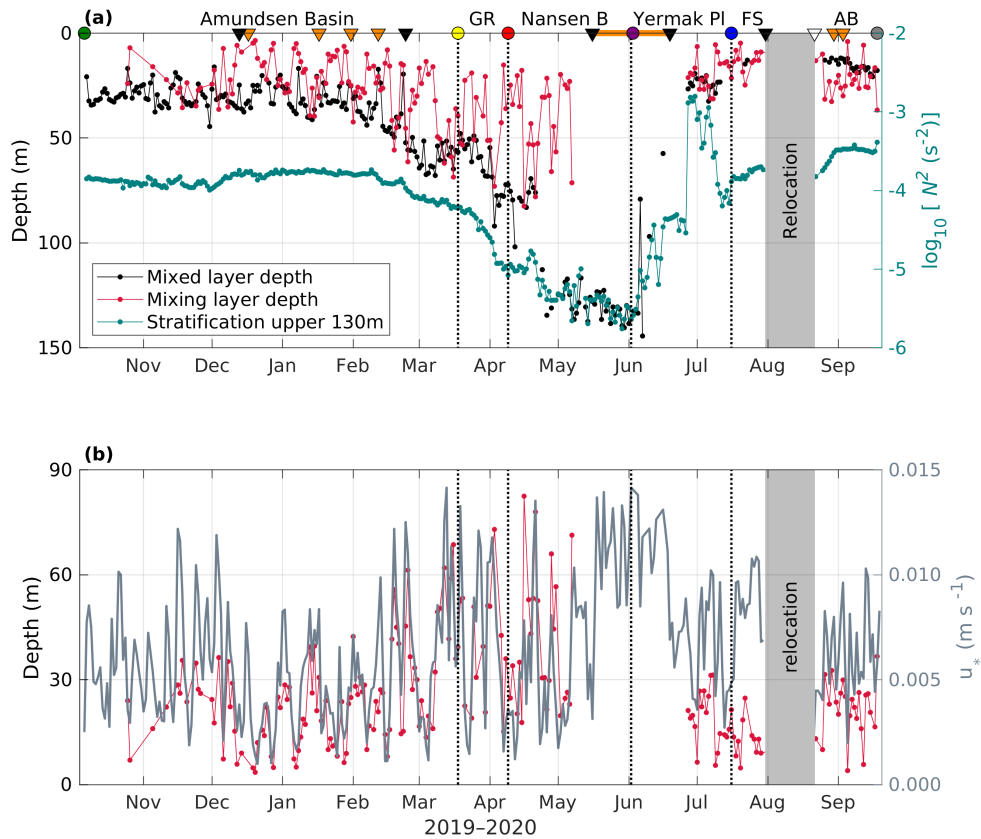


Figure 6. Parameters related to surface turbulence along the drift.

(a) Surface mixed layer depth (black) and mixing layer depth (red, m, left vertical axis) and upper ocean stratification (teal, right axis, s^{-2}). (b) Mixing layer depth (red, m, left axis; note that the vertical axis is reversed) and friction velocity (gray, right axis). In (a), black and white triangles indicate the start and end of the legs, dots, vertical dotted lines and annotations the geographical markers including Amundsen Basin (AB), Gakkkel Ridge (GR), Nansen Basin (B), Yermak Plateau (PI) and Fram Strait (FS). The orange line indicates the uncrewed period of the drift as in Figure 1b and orange triangles indicate near surface eddies.

633 forces, such as strong lateral gradients. This delay explains why the distribution
634 of biological and biogeochemical tracers is often homogeneous in the actively
635 mixing layer, but not in the mixed layer, where it instead reflects a combined sig-
636 nal of past active mixing and new biological production (or consumption) in the
637 respective layers (Carranza et al., 2018).

638 The relation between the depth of the mixed layer and depth of the active
639 mixing layer is illustrated in Figure 6a. At times during MOSAiC, active mixing
640 reached down to the base of the mixed layer, but was often confined to the upper
641 20 m. In the Nansen Basin, in the presence of deep ventilation conditions, active
642 mixing occasionally reached to a maximum depth of 80 m, but not to the mixed
643 layer base located at approximately 130 m. However, we have limited observations
644 of turbulence here, due to the interruption of the drift between Legs 3 and 4. Upon
645 return to the Amundsen Basin in summer, the mixed layer depth was shallower
646 compared to the winter condition, caused by a lower surface salinity and hence
647 stronger upper ocean stratification (teal line; Figure 6a). The active mixing layer
648 depth, however, is comparable to the maximum depth of active mixing typically
649 observed in this region in winter, during the first part of the drift, and reaches
650 *deeper* than the mixed layer base. In other words, the same level of turbulent
651 energy that created an approximately 30 m deep mixed layer in the presence of
652 weaker upper ocean stratification (first part of the drift), only created a 20 m deep
653 mixed layer in the presence of stronger stratification (last part of the drift). This
654 comparison illustrates how strong stratification requires more turbulent energy to
655 be mixed and that storm events, associated with elevated levels of turbulence,
656 can have a different impact on the vertical transport of, e.g., nutrients and other
657 biogeochemical compounds or organisms, depending on the strength of the upper
658 ocean stratification.

659 As the turbulent energy in the mixing layer mainly originates from friction at
660 the ice-ocean interface, the depth of the mixing layer is, to a large extent, related
661 to the sea ice drift speed. A parameter to describe the impact of drift speed on
662 upper ocean turbulence is the friction velocity, u_* (right vertical axis in Figure 6b).
663 In the (winter) Amundsen Basin and in the Nansen Basin, the evolution of the
664 mixing layer depth corresponds to variations in friction velocity, on a daily time
665 scale. The relationship is different, but still visible, above the Yermak Plateau
666 and breaks down in Fram Strait. Both regions were characterized by considerably
667 higher current velocities, which likely contributed to the friction at the ice-ocean
668 interface. Furthermore, sea ice melt probably reduced the bottom roughness of the
669 sea ice (which was kept constant in the u_* calculation here), thereby reducing the
670 efficiency of energy transfer from sea ice drift to surface ocean turbulence. After

671 resuming sampling on another ice floe in the Amundsen Basin in late summer, in
672 the presence of a stronger upper ocean stratification, the mixing layer depth was
673 relatively constant and the effect of the friction velocity less clear. In summary,
674 variations in ice drift speed strongly influenced the mixing layer depth on daily or
675 probably shorter time scales, but other effects like the upper ocean stratification
676 and tides are likely to alter this relationship.

677 The different timescales on which the active mixing depth and the mixed layer
678 depth vary can have implications for the distribution of tracers and organisms in
679 the near-surface layer. During longer calm periods, when the wind and drift speed
680 are low, vertical biogeochemical gradients might be established within the sur-
681 face mixed layer, e.g., if nutrients are preferentially consumed in the upper part
682 of the mixed layer, where more sunlight is available, or if tracers and organisms
683 from melting sea ice are injected to the ocean and accumulate only in the very top
684 layer. A wind event could then easily homogenize these gradients on very short
685 (hourly) timescales, altering the biogeochemical signature over the whole mixed
686 layer depth. Such an event could boost primary productivity, by replenishing sur-
687 face nutrients, but could also have an adverse effect by displacing organisms to
688 greater depths, where less sunlight is available and food is more diluted.

689 6.2. *Turbulent diffusivity*

690 The decay of turbulent energy with increasing distance from the surface, where
691 it is generated mainly by friction under the sea ice, is visible in Figure 7a. In
692 the Amundsen Basin, strong stratification (Figure 7b) confined elevated levels of
693 mixing to the upper approximately 70 m in winter and, due to stronger surface
694 stratification, to approximately 50 m in summer. In the Nansen Basin, where the
695 upper ocean was well mixed or only weakly stratified (yellow lines in Figure 7),
696 turbulence was elevated in the upper 90 m and still slightly above noise level down
697 to approximately 200 m. The Yermak Plateau and Fram Strait regions were more
698 stratified, partly due to buoyancy input by meltwater and solar warming, but also
699 more dynamic (see Section 5). Here, turbulence was strongly elevated in the upper
700 40 m and still elevated below, though weaker than in the Nansen Basin.

701 Vertical diffusivity, the coefficient necessary to calculate turbulent vertical
702 fluxes in the presence of stratification, differed both regionally and depending
703 on the vertical position in the water column. In the strongly stratified halocline
704 in the Amundsen Basin, values are smallest and on the order of $10^{-6} \text{ m}^2 \text{ s}^{-1}$, as
705 already reported in Schulz et al. (2023a), illustrating how the halocline separates
706 the surface from the deeper water layers. In the conditions we encountered in

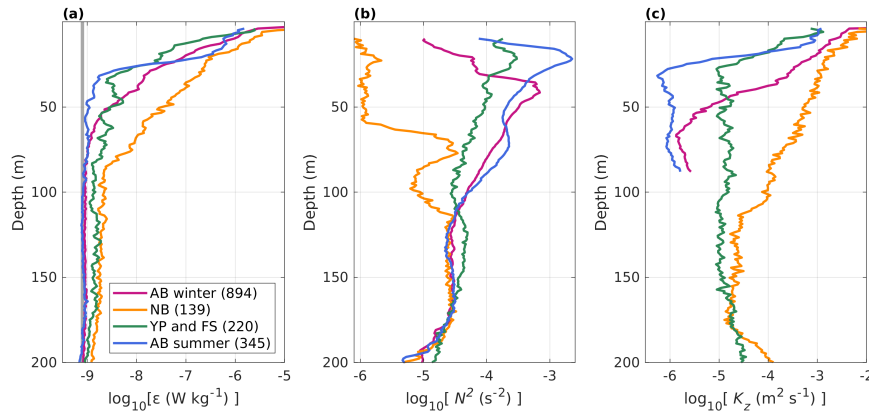


Figure 7. Turbulence and stratification profiles.

Basin-averaged vertical profiles of the (a) turbulent dissipation rate ϵ (W kg⁻¹), (b) Brunt-Väisälä frequency, N , squared (s⁻²) and (c) vertical diffusivity K_z (m² s⁻¹). Colors refer to the Amundsen Basin (AB) summer and winter conditions, Nansen Basin (NB) and the Yermak Plateau (YP) and Fram Strait (FS) averages, the vertical gray line in (a) indicates the lowest detection (“noise”) level of the profiler. Data below around 90 m in the Amundsen Basin and below 200 m in the Nansen Basin and the Yermak Plateau and Fram Strait regions are at noise level and not shown in (c).

707 summer, characterized by lower surface salinity and a shallower mixed layer, the
 708 “bottleneck” for vertical transport formed by the halocline was even more pro-
 709 nounced (blue and violet lines in Figure 7c). In the Yermak Plateau and Fram
 710 Strait regions, upper ocean (30–160 m) vertical diffusivity was an order of mag-
 711 nitude higher, around 10⁻⁵ m² s⁻¹ (green line in Figure 7c). In the Nansen
 712 Basin, upper ocean vertical diffusivity is highest, ranging from more than 10⁻³ m² s⁻¹ in
 713 the upper 50 m and gradually decreasing to approximately 10⁻⁵ m² s⁻¹ at around
 714 170 m depth. Highest vertical fluxes of any tracer, e.g., heat, nutrients or oxygen,
 715 can therefore be expected in the Nansen Basin.

716 The variability within both basins was relatively low, with average values
 717 providing a good representation of the typical conditions. However, the Yermak
 718 Plateau and Fram Strait regions are energetic and exhibited considerably different
 719 conditions, e.g., with respect to tidal currents (Section 5), stratification and At-
 720 lantic Water layer properties (Section 4). Here, average values can be informative
 721 and descriptive, but for detailed studies in those regions, the actual contempora-

722 neous conditions need to be considered.

723 6.3. *Heat fluxes*

724 Ocean heat fluxes presented here were calculated in two ways. Close to the surface
725 (3 m depth), high-resolution point measurements of three-dimensional velocity
726 and temperature from an autonomous buoy provided heat fluxes based on direct
727 eddy correlation methods. In deeper layers, we derived heat fluxes from vertical
728 temperature gradients and the vertical diffusion coefficient K_z (described above),
729 e.g., over the halocline or the Atlantic Water thermocline (see Section 2, Text S1).
730 The heat flux at 3 m reflects how a small difference in heat, i.e., water even slightly
731 above the local salinity-controlled freezing point, is transported near the ice-ocean
732 interface. The heat flux over the halocline describes the heat entering the surface
733 mixed layer from the ocean below. The heat flux over the thermocline can be
734 interpreted as the heat lost from the Atlantic Water to the colder water layer above
735 (Schulz et al., 2021). Similarly, vertical fluxes of other tracers, e.g., nutrients or
736 dissolved oxygen, could be calculated from the K_z data presented here and the
737 respective tracer profiles. Depending on the position of the layer of interest, e.g.,
738 the nitracline, we expect that these fluxes qualitatively follow the variability we
739 observed in heat fluxes.

740 Heat fluxes at 3 m depth, near the top of the ocean mixed layer (Figure 8a),
741 ranged between -2 W m^{-2} and 7 W m^{-2} , exhibiting a typical wide day-to-day
742 variability, arising primarily from the variable wind-forced motion of the ice (Fig-
743 ure 5a). During the winter period, in the absence of solar heating, the 3 m fluxes
744 arose from wind-ice-forced turbulent mixing of heat within the mixed layer and
745 heat trapped by the strong salinity-controlled density gradient at the base of the
746 mixed layer. Heat transport from the base of the mixed layer was strongly am-
747 plified in the presence of eddies. During the ice growth period (December to end
748 of April), ice basal growth of 0.92 m to 1.05 m was measured (AOFB altimeter
749 on a different floe; Perovich et al., 2023). This basal growth is dominated by ice
750 conductive fluxes controlled by air temperature, humidity, wind speed, the effects
751 of highly insulating snow, ice thickness and ice salinity. Because the ocean mixed
752 layer temperature is very close to the freezing point (Figure 4b; Section 4.2), heat
753 lost to the ice cannot further cool the ocean, but rather forms ice, releasing brine
754 and removing latent heat from the ice-water interface (e.g., McPhee, 2008). The
755 small contribution to ice basal change from time-integrated predominantly upward
756 heat fluxes for this time series was just 1.2 cm of ice loss, with little contribution
757 after the beginning of May 2020.

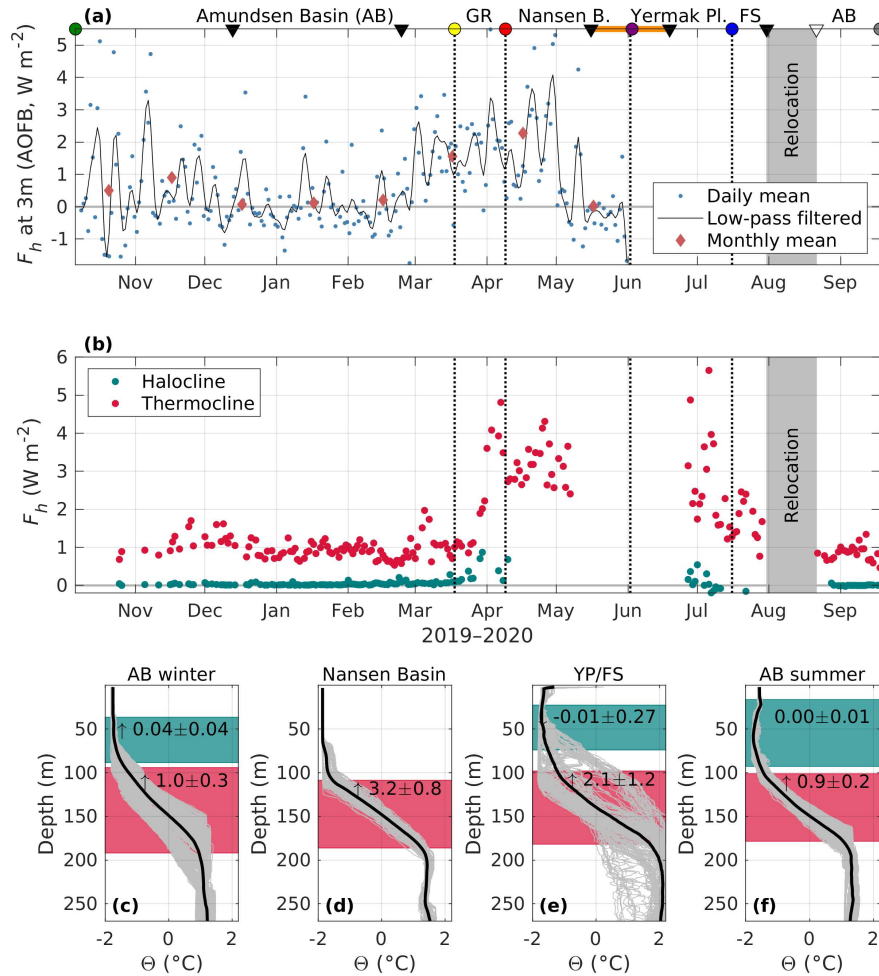


Figure 8. Vertical heat fluxes during the drift.

(a) Heat fluxes (F_h) at 3 m depth, based on eddy-correlation, measured with an Autonomous Ocean Flux Buoy at the Distributed Network "L2" site (Rabe et al., 2022), at a distance of 15–25 km from *Polarstern*. Blue dots are daily averages; the black line is a 6-day low-pass filtered time series and red diamonds are monthly mean flux values. (b) Heat fluxes over the halocline (teal dots) and Atlantic Water thermocline (red dots) based on shear probe measurements. (c-f) Individual (gray) and average (black) conservative temperature (Θ) profiles and average halocline and thermocline heat fluxes in the Amundsen Basin (AB) in summer and winter, the Nansen Basin and the Yermak Plateau and Fram Strait regions (YP/FS). All values are in W m^{-2} . In (a), triangles indicate the start and end of the legs; dots, vertical dotted lines; and annotations, the geographical markers including the Gakkel Ridge (GR), Nansen Basin (B), Yermak Plateau (Pl) and Fram Strait (FS). The orange line indicates the uncrewed period of the drift as in Figure 1b.

758 As previously reported, based on the winter Amundsen Basin data from MO-
759 SAiC (Schulz et al., 2023a), the heat flux over the halocline is negligible, meaning
760 that the halocline effectively shelters the upper water layers and the sea ice from
761 the heat in the Atlantic Water layer. While there was a minimal upward flux in the
762 Amundsen Basin in winter, with heat fluxes much smaller than 0.1 W m^{-2} , the
763 stronger stratification present in summer completely suppressed any heat trans-
764 port over the halocline (Figure 8a,c,f). As the Gakkel Ridge was approached in
765 March, halocline heat fluxes gradually increased, reaching maximum levels above
766 the ridge. However, daily mean values were still small, below 0.8 W m^{-2} (directed
767 upwards). Halocline heat fluxes above the Yermak Plateau were comparable to
768 those above the Gakkel Ridge, until surface heating reversed the temperature gra-
769 dient and small, downward-oriented heat fluxes were observed.

770 Upward heat loss from the Atlantic Water layer in the Amundsen Basin was
771 around 1 W m^{-2} , with little (sub)seasonal variability. Under deep ventilation con-
772 ditions in the Nansen Basin, in the absence of a sheltering halocline, the more
773 turbulent surface layer directly connects with the Atlantic Water layer and ther-
774 mocline heat fluxes increased by a factor of three, compared to the Amundsen
775 Basin conditions with a stable halocline (Figure 8b,c,d,f). In the Yermak Plateau
776 and Fram Strait regions, heat fluxes were also enhanced, but the temperature struc-
777 ture in the water column, and hence the heat flux, was more variable (Figure 8c).
778 Here, heat fluxes were highest on the plateau, where the Atlantic Water layer is
779 shallow and the Atlantic Water core is warmer (and younger) compared to the rest
780 of the drift. Heat fluxes decreased to a level between Nansen and Amundsen Basin
781 conditions as Fram Strait was entered.

782 7. Comparison of MOSAiC data and ocean climatologies

783 Ocean climatologies are interpolations of observed temperature and salinity pro-
784 files, which are often used as initial or boundary conditions in modeling studies,
785 or for ground-truthing the results of simulations. In contrast, state estimates are
786 realizations of numerical models that have been optimized to best fit observa-
787 tional data, while obeying the physical laws that govern processes in the ocean.
788 The majority of data used to create the climatologies were collected more than 10
789 years ago (Table 1). Because the Arctic is the world’s fastest-changing region, it is
790 unclear how representative these datasets still are. The high-resolution MOSAiC
791 data can serve as a benchmark for the “modern-day” Eurasian Arctic, enabling an
792 evaluation of how representative the climatologies are of the current conditions.
793 Here, we compare four climatologies and two state estimates in three time periods/

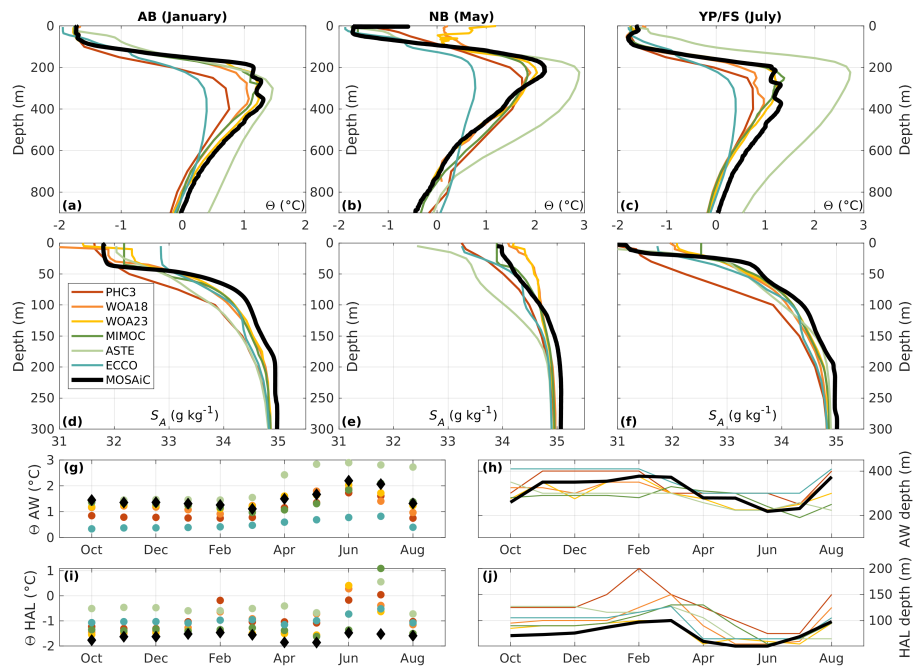


Figure 9. Comparison of the observations along the drift with climatological datasets and state estimates.

(a-c) Conservative temperature (Θ) and (d-f) absolute salinity profiles of four climatological datasets (PHC3, WOA18, WOA23 and MIMOC) and two state estimates (ECCO and ASTE; see Section 2 and Text S1 for definitions and details) and the MOSAIC observations. Note the different ranges on the y-axis for salinity and temperature. Data have been averaged for the months of January in the Amundsen Basin (AB), May in the Nansen Basin (NB) and July in the Yermak Plateau and Fram Strait regions (YP/NB). (g) Atlantic Water (AW) core conservative temperature (Θ) and (h) depth (m), and (i) halocline (HAL) conservative temperature (Θ) and (j) depth (m).

794 regions (Figure 9) to the new MOSAiC data. We calculated month-long averages
795 of the MOSAiC data, with the January average representing Amundsen Basin
796 winter conditions, May representing spring conditions in the Nansen Basin, and
797 July representing summer conditions in the Fram Strait region. The correspond-
798 ing climatological averages were derived from the objectively analyzed monthly
799 datasets of each climatology/state estimate, utilizing the nearest climatology grid
800 cell to the drift location at the midpoint of the corresponding month. For additional
801 information, including details about the respective data sources for the climatolo-
802 gies, see Text S1.

803 Overall, we found good agreement between the climatologies and MOSAiC
804 data, regarding the vertical structure and seasonal and regional variability. The
805 MIMOC and WOA18 climatology show strong agreement and similarity, despite
806 WOA18 containing a larger proportion of older data compared to MIMOC. The
807 two state estimates, ECCO and ASTE, accurately reconstruct the complex ver-
808 tical structure and the halocline, as well as seasonal and regional changes. Not
809 all climatologies accurately represent the surface mixed layer, which is subject to
810 considerable short-term variability, as profiles were often averaged over different
811 regions and time periods. MIMOC is the only climatology that considers this issue
812 during the interpolation and objective mapping process.

813 PHC3, with the oldest data of all the data products considered here (Table 1),
814 features a fresher Atlantic layer and halocline, compared to other data prod-
815 ucts and MOSAiC data, which is expected as most data are pre-Atlantification
816 (Polyakov et al., 2017). The state estimates ECCO and ASTE are subject to tem-
817 perature biases in the Atlantic layer, with ECCO being 1–1.5°C colder and ASTE
818 being 0.2–2.0°C warmer (with a larger bias in spring/summer Eurasian Basin than
819 in the winter Amundsen Basin), compared to the observed Atlantic Water core.
820 ASTE also exhibits a salinity bias, with a fresher Atlantic Water and halocline
821 layer, resulting in a weaker stratification. These biases point to issues reproducing
822 the Atlantic Water pathway (a common issue in many models, e.g., Heuzé et al.,
823 2023b; Wang et al., 2023), an underestimation of vertical heat fluxes from the At-
824 lantic Water layer and not enough observations along the Eastern Arctic boundary
825 current available to constrain the model (Nguyen et al., 2021). Constraining a new
826 release of ASTE with MOSAiC data will likely reduce this bias.

827 Across all basins and seasons, the MOSAiC data consistently exhibit warmer
828 Atlantic Water, compared to the climatologies. The climatologies demonstrate a
829 clear temporal dependency, with PH3, containing the oldest data, featuring the
830 coldest Atlantic Water, approximately 1°C colder compared to the most recent
831 WOA23. This observation aligns with the expected consequences of rapid Arctic

832 Amplification and Arctic Ocean warming (Rantanen et al., 2022). Another pos-
833 sible shift is indicated in the Amundsen Basin halocline properties, the extent of
834 which decreases from 130–200 m in the (oldest) PHC3 climatology to 70–100 m
835 during MOSAiC. This shift is in line with previous findings of a weakening and
836 shallowing of the halocline over recent decades (Polyakov et al., 2020a).

837 However, MOSAiC data comprise a snapshot of only one year and do not
838 capture interannual or decadal variability (e.g., Polyakov et al., 2023). The identi-
839 fication of long-term variability and/or climate-change-induced changes in water
840 mass properties at all depths is not trivial. It requires in-depth analyses of variabil-
841 ity and changes in both the upstream (e.g., properties in and exchanges with the
842 Nordic Seas) and the internal (e.g., shelf ventilation) processes. Such analyses can
843 only be undertaken by comparing MOSAiC to several decades of scarce, historical
844 data and are beyond the scope of this study. We also note that, consistent with
845 previous studies (e.g., Timmermans and Marshall, 2020), we observed significant
846 regional disparities within the Arctic Ocean, surpassing temporal variations on
847 both short and long-term timescales. Therefore, while the MOSAiC data reflect
848 conditions in the Eurasian basins, they do not necessarily represent modern-day
849 conditions elsewhere in the Arctic (see also Section 9).

850 8. Discussion

851 8.1. *MOSAiC findings in comparison with previous results*

852 8.1.1. Surface waters

853 Upper ocean properties along the MOSAiC drift were strongly influenced by the
854 relative position of the sampling within or outside of the river water-rich Trans-
855 polar Drift. A direct comparison to earlier observations is challenging, as the ex-
856 act pathway of river water is subject to seasonal and interannual variability (e.g.,
857 Mysak, 2001; Karcher et al., 2012) and sampling locations of previous expedi-
858 tions or ITP drift tracks differ from the MOSAiC locations. At the beginning
859 of the MOSAiC drift, the mixed layer salinity in the eastern Amundsen Basin,
860 around 32 g kg^{-1} (Figure 4b), appears to be higher than in the early 2010s in
861 the same area: Observations from late summer in 2011 (*Polarstern* expedition
862 PS78; Gonçalves-Araujo et al., 2018) and 2012 (ITP64; Stedmon et al., 2021)
863 show a fresher surface layer with salinity around 30 g kg^{-1} and a higher CDOM
864 loading, indicative of larger presence of river runoff in the easternmost Amund-
865 sen basin. Similar conditions were observed in 2015 (*Polarstern* expedition PS94;
866 Stedmon et al., 2021). This difference in surface salinity and CDOM concentra-
867 tion might indicate that the first part of the MOSAiC drift was rather intersecting

868 the "edge" of the river water-rich Transpolar Drift and not the core, where surface
869 salinity would likely be closer to 30 g kg^{-1} , at least in late summer, and river
870 water fraction would be closer to 20% (e.g., Bauch et al., 2011; Charette et al.,
871 2020; Paffrath et al., 2021). The conditions observed after re-location closer to
872 the North Pole (where the freshwater-rich part of the Transpolar Drift is often lo-
873 cated), with surface salinities around 29 g kg^{-1} (Figure 4b), are more typical for
874 the freshwater-rich part of the Transpolar Drift (e.g., Bauch et al., 2011; Charette
875 et al., 2020). Provenance tracer data show that the river water component of the
876 freshwater-rich part has a considerable proportion of Lena River water, while the
877 lower river water fractions at the "edges" are mainly attributable to contributions
878 from the Yenisei and Ob rivers (G Laukert, unpublished). These attributions are
879 consistent with a shorter advection time of Lena River water into the central Arctic
880 Ocean, resulting in less mixing with ambient water, and suggests significant differ-
881 ences in biogeochemical water properties even within the river water-influenced
882 part of the Transpolar Drift.

883 8.1.2. Surface mixed layer depth

884 Peralta-Ferriz and Woodgate (2015) reported estimates of the mixed layer depth
885 for the whole Eurasian Basin, using 519 profiles in the time period 1979–2012.
886 Based on monthly averages, they found a maximum mixed layer depth of 73 m in
887 April, but also observed depths of $>100 \text{ m}$ in winter and a minimum depth of 22 m
888 in July/August. These ranges are similar to the conditions encountered during
889 MOSAiC, given the high internal variability of the mixed layer depth. Peralta-
890 Ferriz and Woodgate (2015) also highlighted that the Arctic mixed layer depth
891 distribution is patchy and found a dominance of upper ocean stratification, rather
892 than wind or drift speed, in determining the local mixed layer depth in ice-covered
893 situations. Throughout the MOSAiC drift, we also found the mixed layer depth to
894 be influenced strongly by the surface salinity, which to first order sets the upper
895 ocean stratification. In the presence of a surface salinity below 30 g kg^{-1} , the
896 maximum mixed layer depth was just over 20 m (Amundsen Basin, summer),
897 whereas at a higher surface salinity of around 32 g kg^{-1} the surface mixed layer
898 was as deep as 50 m. Deep ventilation, with a mixed layer depth of around 130 m,
899 was observed only at a surface salinity greater than 34.1 g kg^{-1} (Nansen Basin).
900 Winter deep ventilation has been observed previously (Polyakov et al., 2017) and
901 was attributed to changes associated with Atlantification, e.g., weakened upper
902 ocean stratification, higher turbulence and enhanced heat fluxes. MOSAiC data
903 show that these conditions were present everywhere along the drift track in the
904 Nansen Basin. However, a similar disappearance of the halocline, related to a

905 high surface salinity, was already observed in the eastern Arctic Ocean in the
906 1990s (Steele and Boyd, 1998) and found to be transient (Boyd et al., 2002).

907 8.1.3. Halocline thickness and stratification

908 Based on 18,000 profiles of ocean temperature and salinity collected during the
909 period 1997–2008, Bourgain and Gascard (2011) assessed properties of the Arc-
910 tic halocline. Similar to the variability encountered during MOSAiC, they found
911 the strongest, i.e., most stratified, halocline layers close to the freshwater sources
912 at the Siberian shelves. The weakest haloclines (together with the deepest mixed
913 layers, down to 70 m) were found in the western Nansen Basin, where we encoun-
914 tered a deeper mixed layer and a complete absence of the halocline during MO-
915 SAiC. Bourgain and Gascard (2011) found the halocline in the Amundsen Basin
916 to be very stable during their investigated time period, with no clear seasonal vari-
917 ability, but their data coverage in winter was sparse. During MOSAiC, we found
918 an apparent seasonal signal, with a thicker (76 ± 9 m versus 50 ± 11 m) and more
919 stratified ($50 \pm 7 \times 10^{-5} \text{ s}^{-2}$ versus $28 \pm 8 \times 10^{-5} \text{ s}^{-2}$) halocline in summer,
920 compared to the winter situation, which is attributed to a lower surface salinity in
921 summer. However, while seasonal meltwater in the surface layer has an effect on
922 the surface salinity, MOSAiC data indicate that the local surface salinity is set by
923 the relative position within or outside the river-water influenced Transpolar Drift
924 rather than by seasonality (see Section 4). Taking into account both seasons, the
925 Amundsen Basin halocline got thinner (55 ± 14 m versus 70 ± 10 m) but more
926 stratified ($32 \pm 12 \times 10^{-5} \text{ s}^{-2}$ versus $20 \pm 3 \times 10^{-5} \text{ s}^{-2}$) compared to the values
927 reported in Bourgain and Gascard (2011). Given the strong spatial gradients in
928 surface salinity in the Amundsen Basin and the still limited spatial coverage of
929 data, these differences could reflect internal variability rather than trends.

930 8.1.4. Heat fluxes

931 Heat fluxes near the ice-ocean interface (at a depth of 3 m) exhibited low val-
932 ues during the MOSAiC winter and displayed significant day-to-day fluctuations.
933 This pattern aligns with the findings of Meyer et al. (2017a) in the Nansen Basin
934 during the N-ICE2015 winter (at 1 m depth). Moving into early spring, specifi-
935 cally in May, the heat fluxes recorded by the AOFB buoy reached levels of around
936 5 W m^{-2} , a value that is consistent with the approximately 10 W m^{-2} reported
937 by Meyer et al. (2017a) for the same month. In June, during the N-ICE2015 cam-
938 paign, the fluxes ranged over $10\text{--}50 \text{ W m}^{-2}$, reaching peaks exceeding 300 W m^{-2}
939 during storms that caused upward mixing of warm subsurface waters. Unfortu-
940 nately, the MOSAiC data lack shallow measurements from June onwards.

941 Heat fluxes across the halocline during MOSAiC were virtually zero, which is
942 in line with previous findings (Fer, 2009), including from the SHEBA campaign in
943 the Western Arctic (Shaw and Stanton, 2014). Also, the relatively low heat fluxes
944 over the Atlantic Water thermocline found in Amundsen Basin match previously
945 reported values in that region (Lenn et al., 2009; Schulz et al., 2021). The higher
946 heat fluxes over the thermocline found in the Nansen Basin correspond to values of
947 around 3 W m^{-2} found during N-ICE2015 (Meyer et al., 2017a) and elevated heat
948 fluxes in the absence of a halocline, as observed in the Nansen Basin, have been
949 reported previously (Steele and Boyd, 1998). Heat fluxes over the thermocline for
950 June and July were generally confined to the range of $2\text{--}5 \text{ W m}^{-2}$; much lower
951 than during N-ICE2015. This limited range is attributed primarily to the shallower
952 warm Atlantic layer in the N-ICE2015 area compared to the MOSAiC location
953 and the absence of storms during this period of the MOSAiC drift.

954 8.2. *Interdisciplinary implications*

955 The regional differences in physical hydrography encountered during the MO-
956 SAiC drift have various implications for other Arctic subsystems. In the follow-
957 ing, we discuss how the variability in physical properties along the MOSAiC drift
958 might shape the distribution of nutrients and the carbonate system, bio-optical
959 properties, the ecological structure across multiple trophic levels and sea ice and
960 atmospheric processes.

961 8.2.1. Nutrient and carbonate system dynamics

962 Water masses, transport and turbulent mixing impact the distribution of nutrients,
963 carbon and other geochemical tracers. Nutrient inventories in the surface waters
964 differ regionally, with signals being potentially larger than the seasonal signals
965 of biological uptake and remineralization (Juranek, 2022), particularly in basins
966 with longer ice-cover duration where the residence time of tracers is increased
967 due to accumulation in surface waters (Eveleth et al., 2014). Similarly, for vari-
968 ous carbonate system components, such as dissolved inorganic carbon (DIC) and
969 total alkalinity (TA), a strong positive correlation is usually found with salinity
970 (Friis et al., 2003), indicating that the marine carbonate system is closely related
971 to physical water mass properties.

972 Atlantic Water, residing at depths greater than 100 m, forms the largest source
973 of nutrients in the central Arctic Ocean and is an enormous reservoir of dissolved
974 inorganic carbon (DIC), as organic matter from the sun-lit surface ocean eventu-
975 ally sinks and remineralizes. The transport of these nutrients and carbon up to the

976 photic zone, where they can be utilized by primary producers, is strongly limited
977 by the presence of the halocline, which acts as a barrier layer (e.g., Fer, 2009;
978 Schulz et al., 2022a). When the halocline is absent and the mixed layer penetrates
979 the Atlantic Water layer (Polyakov et al., 2017), ventilation can potentially create
980 locally larger nutrient inventories at the start of the productive season and enhance
981 the biological carbon drawdown (Juraneck, 2022). These physical conditions were
982 observed in the Nansen Basin (Section 4.2). Enhanced vertical nutrient transport
983 might also occur when Atlantic Water resides high up in the water column (as on
984 the Yermak Plateau; Section 4.3). On the other hand, vertical mixing of deep DIC
985 during ventilation or passing eddies, can partially offset biological CO₂ drawdown
986 by increasing the partial pressure of CO₂ (pCO₂) in the surface layer (Bates and
987 Mathis, 2009; Lannuzel et al., 2020).

988 Among marine carbonate system components, the surface layer pCO₂ is often
989 the point of focus in sea-air CO₂ exchange studies, as it determines whether the
990 ocean is a sink or source of CO₂ to the atmosphere. The Arctic Ocean is generally
991 considered to be a CO₂ sink, as surface layer pCO₂ is often undersaturated relative
992 to the atmosphere (Tanhua et al., 2009; Schuster et al., 2013; Fransson et al., 2017;
993 Rogge et al., 2023). Arctic Ocean pCO₂ undersaturation is driven by low seawater
994 temperatures, sea ice meltwater input, biological CO₂ uptake during the summer
995 and strong upper ocean stratification (Bates et al., 2006; Takahashi et al., 2009;
996 Fransson et al., 2017). In addition to the variability in the Arctic Ocean's nutri-
997 ent content and capacity to absorb atmospheric pCO₂ driven by biogeochemical
998 and sea ice processes, physical processes also can lead to changes in the marine
999 nutrient and carbonate system on short time scales. For example, frontal regions
1000 are associated with enhanced biological activity, leading to variability in uptake
1001 and remineralization rates of nutrients across smaller hydrographic scales (Eveleth
1002 et al., 2014). Tidal currents in regions where horizontal gradients of water masses
1003 exist, e.g., between the Yermak Plateau and Fram Strait, can also lead to rapid
1004 change in the nutrient and carbonate system of the surface ocean on semidiurnal
1005 and diurnal time scales and cause polar waters to switch between a CO₂ sink and
1006 source multiple times a day (Skogseth et al., 2013; Llanillo et al., 2019; Droste
1007 et al., 2022).

1008 8.2.2. Optical properties

1009 The optical properties of the surface waters of the MOSAiC exhibited regional
1010 differences between the basins, exemplified by the documented differences in
1011 CDOM concentrations, with elevated concentration when in the Transpolar Drift
1012 (see Section 4.2). In Arctic waters, CDOM is an important factor of light attenua-

1013 tion in the water column (e.g., Hill, 2008; Granskog et al., 2007; Pavlov et al.,
1014 2015) and varies regionally, largely depending on the presence of river water.
1015 The presence of river water divides the Eurasian basin into bio-optical provinces
1016 (Gonçalves-Araujo et al., 2018), which has implications for light availability for
1017 primary producers (e.g., Pavlov et al., 2015), especially in the absence of sea ice.
1018 Solar heating of the upper ocean is also affected by the distribution of CDOM
1019 (Hill, 2008; Granskog et al., 2015) and could thus affect sea ice melting across
1020 regimes.

1021 8.2.3. Ecology

1022 Regional variability in both nutrient concentrations and the optical regime can
1023 induce compositional changes to the microbial community, with complex impli-
1024 cations for the carbon biogeochemistry. For example, increased vertical transport
1025 of nutrients from the deep ventilation observed in the Nansen Basin could lead
1026 to a shift from smaller to larger phytoplankton, while increased stratification and
1027 warming can lead to opposite trends (Li et al., 2009; Morán et al., 2010). Addi-
1028 tionally, hydrographic boundaries can act as physical barriers limiting dispersal,
1029 resulting in vertical and biogeographic differences in microbial diversity and com-
1030 munity structure among water masses and basins (Galand et al., 2010; Han et al.,
1031 2015). During MOSAiC, unique upper water column microbial community com-
1032 positions were indeed observed when crossing boundaries such as the base of the
1033 mixed layer, or when drifting into and out of the Transpolar Drift (EJ Chamber-
1034 lain, unpublished). A key driver in regional differences in Arctic Ocean bacterial
1035 communities is the relative proportion of Atlantic water influence, with species
1036 composition and ecological function, i.e., substrate utilization, responding rapidly
1037 to changes in the environmental regime. This connection makes the variability in
1038 water masses, for example the high relative proportion of Atlantic water observed
1039 while crossing the Yermak Plateau, a key driver in regional differences of micro-
1040 bial communities (Carter-Gates et al., 2020; Priest et al., 2023). At higher trophic
1041 levels, larger boreal species such as fish or squid can enter the Arctic Ocean within
1042 the Atlantic Water layer and appear to survive in parts of the central Arctic. Dur-
1043 ing MOSAiC, healthy Atlantic cod were found in the Amundsen Basin, where a
1044 deep scattering layer indicated the presence of living organisms as food supply
1045 (Snoeijs-Leijonmalm et al., 2022). In the Nansen Basin, this deep scattering layer
1046 was absent and fish and squid abundance decreased. The inflow region of young
1047 Atlantic Water near the Yermak Plateau, on the other hand, was characterized by
1048 large aggregations of Atlantic fish species (Snoeijs-Leijonmalm et al., 2022).

1049 8.2.4. Sea ice and atmosphere

1050 Oceanic heat, when reaching the surface, affects sea ice growth and melt. Dur-
1051 ing MOSAiC, the sea ice basal growth was found to transition from a rapid to a
1052 slower growth rate, when drifting from Amundsen Basin to Nansen Basin (Lei
1053 et al., 2022). This change in basal growth rate might be related, to some extent,
1054 to the greater vertical heat transport from the Atlantic Water layer in the Nansen
1055 Basin, associated with the ventilation conditions (i.e., absence of the halocline;
1056 Polyakov et al., 2017). During the melt season, elevated ocean surface tempera-
1057 tures contribute to sea ice melt and small vertical gradients in upper ocean temper-
1058 ature might set different melt rates at, e.g., ridge keels (Salganik et al., 2023b). The
1059 presence of shallow, strongly stratified meltwater layers also affects sea-ice melt
1060 rates (Salganik et al., 2023a; Smith et al., 2023). Indirectly, even atmospheric con-
1061 ditions might be influenced by surface ocean conditions, by affecting the emission
1062 of marine aerosol precursors that play an important role in, e.g., cloud formation
1063 (Schmale et al., 2021).

1064 9. Summary and outlook

1065 For this study, we compiled a quality-controlled dataset of temperature and salin-
1066 ity profiles and derived parameters, with the best available temporal coverage
1067 along the whole MOSAiC drift across the Eurasian basin in 2019–2020. Derived
1068 core parameters based on this dataset (Table S1; Schulz et al., 2023b; Mieruch,
1069 2023) can be used for interdisciplinary studies aiming to understand interactions
1070 between ocean physical properties and a large range of other measurements con-
1071 ducted during MOSAiC. We find that from an ocean perspective, MOSAiC was
1072 a transect across the Eurasian basin rather than a time series primarily reflecting
1073 a seasonal evolution. Considerable gradients in the surface waters were present,
1074 related to the MOSAiC ice camp drifting into and out of the river water-influenced
1075 Transpolar Drift in the Amundsen Basin. In the Nansen Basin, high surface salin-
1076 ity and the associated absence of the halocline allowed for a more direct connec-
1077 tion and enhanced exchange between the surface and deeper waters of Atlantic
1078 origin. Further south, above the Yermak Plateau and in Fram Strait, oceanic con-
1079 ditions were more dynamic, with a pronounced regime shift back into surface
1080 waters with a high fraction of terrestrial water when leaving the Yermak Plateau.
1081 This spatial variability likely entails large implications for the Arctic Ocean bio-
1082 geochemistry, ecology and even sea ice and atmospheric conditions.

1083 The large regional variability encountered during the drift illustrates that MO-
1084 S AiC results are not representative of the entire Arctic Ocean. Conditions encoun-

1085 tered in the Eurasian deep basins are substantially different from the Amerasian
1086 Basin, where the Beaufort Gyre accumulates large amounts of freshwater and Pa-
1087 cific Water is commonly present in the upper water column. Conditions in the
1088 basins also deviate from the more variable and energetic continental shelf and
1089 slope regions. Furthermore, the observed strong dependence of ocean conditions
1090 on the Transpolar Drift pathway, setting surface salinity, stratification and ver-
1091 tical transport, illustrates that a slight deviation in the ice drift path could have
1092 restricted the range of sampled conditions. For example, if the drift track had not
1093 crossed the Gakkel Ridge and instead had stayed within the cross-Arctic trans-
1094 port pathway of Siberian freshwater, MOSAiC would have missed the ventilation
1095 conditions in the Nansen Basin. The pathway of the Transpolar Drift depends on
1096 large-scale atmospheric forcing and varies on interannual to decadal timescales
1097 (Polyakov et al., 2023). In the period 2007–2021, a positive Arctic Dipole, i.e., rel-
1098 atively higher sea level pressure over the Beaufort Sea and Canadian Archipelago
1099 and lower sea level pressure over the Siberian Arctic, reinforced both the Beau-
1100 fort Gyre and shifted the Transpolar Drift path from the Amerasian Basin toward
1101 the Lomonosov Ridge. Freshwater of Siberian origin accumulated in the Beaufort
1102 Gyre, leading to a stronger salinity stratification in the Amerasian Basin and a
1103 weaker stratification in the Eurasian Basin. The underlying atmospheric forcing
1104 changes on a timescale of approximately 15 years, and superimposes on climatic
1105 trends such as warming Atlantic water and altered freshwater dynamics. For in-
1106 stance, the less pronounced summer sea ice decline since 2007 might originate
1107 from reduced ocean heat transport in the presence of stronger stratification in the
1108 Amerasian Basin created by the positive Arctic Dipole (Polyakov et al., 2023).
1109 The representativeness of MOSAiC results of the annual cycle and for other parts
1110 of the Arctic, especially for the biogeochemical and ecological system, needs to
1111 be assessed with more observations. Nevertheless, the MOSAiC data provide an
1112 important benchmark for detecting future changes in the Eurasian basin.

1113 Future research efforts aiming to monitor climatic trends in the Arctic Ocean
1114 need to account for this large interannual and regional variability, which ideally
1115 requires long time series from stationary moorings and repeated sections/stations,
1116 as well as wide temporal and spatial coverage by autonomous drifting buoys and
1117 floats. Numerical models will be necessary to extrapolate and scale up observa-
1118 tional data, by identifying the spatial extent of distinct oceanographic regimes
1119 (e.g., ventilation conditions in the absence of a halocline, as in Polyakov et al.,
1120 2017, and observed in the Nansen Basin) in response to seasonal and atmospheric
1121 forcing, and process studies will be needed to isolate the respective effect of indi-
1122 vidual driving mechanisms for ocean variability. The strength of MOSAiC lies in

1123 its multidisciplinary approach. MOSAiC observed key parameters simultaneously,
1124 including atmospheric forcing, sea ice and ocean conditions, as well as ocean bio-
1125 geochemistry and ecology, at high temporal sampling frequency and on a range of
1126 scales from manned measurements at the central floe and autonomous platforms
1127 in the surrounding area to remote sensing by aircrafts and satellites. This strategy
1128 has provided unprecedented means to determine connections within the coupled
1129 Arctic system on multiple timescales. Despite the challenges in data interpreta-
1130 tion arising from the overlapping timescales and the superposition of spatial and
1131 temporal signals inherent to a drift campaign, the large variability of conditions
1132 observed during MOSAiC helps us to better understand processes and connec-
1133 tions across the coupled system over timescales from hours to months. MOSAiC
1134 datasets also provide an unprecedented opportunity for the scientific community
1135 to improve the ocean and climate models pivotal to Arctic and Earth system re-
1136 search. Achieving this goal requires dedicated time, effective communication be-
1137 tween observational and modeling communities, and adequate funding.

1138 One final aspect we would like to highlight about the value of MOSAiC for
1139 the polar and climate research community is the high degree of fruitful scientific
1140 collaborations that have been established as a result of this unique experiment. De-
1141 spite or perhaps because of the complexity of and challenges encountered during
1142 the campaign, MOSAiC has created a striving community that has been working
1143 together across disciplines to interpret the collected data, involving an increasing
1144 number of early career scientists. Many of the collaborations and partnerships be-
1145 tween the international partners have been maintained, and even strengthened and
1146 expanded. The project serves as an example of how to foster scientific collabora-
1147 tion and unleash the scientific spirit of a research community. In the end, the true
1148 value of MOSAiC may likely be found beyond the experiment itself.

1149 Data accessibility statement

1150 All datasets used in this study are publicly available, in compliance with the MO-
1151 SAiC data policy. In addition, we published a daily average dataset based on the
1152 2,434 temperature and salinity profiles, as outlined in Text S1, and derived pa-
1153 rameters, as listed in Table S1, in netCDF format (Schulz et al., 2023b). We also
1154 created webODV compliant data files and views (Mieruch, 2023), from which
1155 subsets of data can easily be extracted. We strongly advise that future studies us-
1156 ing the data presented here also cite the respective original datasets listed below.

1157 CO1 GPS buoy: Nicolaus et al. (2021); CTD *Polarstern*: Tippenhauer et al.
1158 (2023b,c); Ocean City CTD: Tippenhauer et al. (2023a,d); MSS: Schulz et al.

1159 (2023c); ITPs (including CDOM data): Toole and Krishfield (2016); PG buoy O4:
1160 Hoppmann et al. (2022); thermosalinograph: Rex et al. (2021a); Haas et al. (2021);
1161 Kanzow et al. (2021); Rex et al. (2021b,c); ADCP: Baumann et al. (2021); AOFB:
1162 Stanton and Shaw (2023).

1163 Author Contributions

1164 Contributed to conception and design: KS, ZK, CJMH, EC, MM, IF, CH, MAG.
1165 Contributed to acquisition of data: KS, ZK, MM, DB, CJMH, ESD, MH, EC,
1166 GL, TS, IF, CH, SK, TB, ST, MAG.
1167 Contributed to analysis and interpretation of data: KS, ZK, MM, DB, CJMH,
1168 ESD, EC, GL, TS, AQ, IF, CH, SK, MV, MAG.
1169 Drafted and/or revised this article: All authors.
1170 Approved the submitted version for publication: All authors.

1171 Acknowledgements

1172 Data used in this manuscript were produced as part of the international Multi-
1173 disciplinary drifting Observatory for the Study of the Arctic Climate (MOSAiC)
1174 project with the tag MOSAiC20192020 and the Project_ID: AWI_PS122_00. The
1175 Ice-Tethered Profiler data were collected and made available by the Ice-Tethered
1176 Profiler Program (Toole et al., 2011; Krishfield et al., 2008) based at the Woods
1177 Hole Oceanographic Institution (<https://www2.who.edu/site/itp/>). We thank all
1178 persons involved in the expedition of the Research Vessel *Polarstern* (Knust,
1179 2017) during MOSAiC in 2019–2020 as listed in the MOSAiC extended acknowl-
1180 edgment Nixdorf et al. (2021). We especially thank everyone involved in the dis-
1181 cussion during the Second MOSAiC Science Conference in Boulder, Colorado,
1182 which motivated this study. We would also like to thank Daniela Ransby (Pan-
1183 gaea) and Christopher Kracha (Arctic Data Center) for their great support with
1184 the data publications. Finally, we like to thank two anonymous reviewers and our
1185 editor, Jody Deming, for dedicating their time and for their positive evaluation of
1186 our manuscript.

1187 Funding

1188 Financial support for KS was available through the German (BMBF) and UK
1189 (NERC) funded PEANUTS-project (grant number 03F0804A) and the NSF
1190 funded projects NSF-AccelNet-2020387 and OPP-1936506. ZK, TB and IF re-
1191 ceived funding through the AROMA (Arctic Ocean mixing processes and ver-
1192 tical fluxes of energy and matter) project by the Research Council of Norway

1193 (grant no 294396). ZK received funding from the Research Council of Norway
1194 through project BREATHE (grant no 325405). MM and MAG were supported
1195 by funding from the European Union's Horizon 2020 research and innovation
1196 programme under grant agreement No 101003826 via project CRiceS (Climate
1197 Relevant interactions and feedbacks: the key role of sea ice and Snow in the polar
1198 and global climate system) and the Research Council of Norway through project
1199 HAVOC (grant no 280292). MAG also acknowledges support from the Hanse-
1200 Wissenschaftskolleg Institute of Advanced Study (Delmenhorst, Germany). MV
1201 was supported through the Changing Arctic Ocean (CAO) program, jointly funded
1202 by the UKRI Natural Environment Research Council (NERC) and the BMBF,
1203 project Advective Pathways of nutrients and key Ecological substances in the
1204 ARctic (APEAR) grants NE/R012865/1, NE/R012865/2 and #03V01461. SK and
1205 CH were supported by the Swedish Research Council (grant 2018-03859 awarded
1206 to CH); participation of SK to MOSAiC was supported by the Swedish Research
1207 Polar Secretariat. ESD was supported by the European Union's Horizon 2020
1208 research and innovation programme under grant agreement no. 821001; partici-
1209 pation of ESD on MOSAiC was supported by the Natural Environment Research
1210 Council (NERC) through the EnvEast Doctoral Training Partnership (grant no.
1211 NE/L002582/1) and the UK Department for Business, Energy and Industrial Strat-
1212 egy (BEIS) through the UK Arctic Office. TS and the AOFB measurements are
1213 funded by NSF OPP-1723400. GL also gratefully acknowledges financial support
1214 from the Ocean Frontier Institute, supported by a Canada First Research Excel-
1215 lence Fund award (grant no. 39291), and from the European Union's Horizon 2020
1216 research and innovation program under a Marie Skłodowska-Curie Postdoctoral
1217 Global Fellowship award (grant no. 101023769).

1218 Competing interests

1219 All authors declare that they have no competing interests.

1220 References

- 1221 Arrigo, KR, van Dijken, GL. 2015. Continued increases in Arctic Ocean
1222 primary production. *Progress in Oceanography* **136**: 60–70. doi:
1223 <https://doi.org/10.1016/j.pocean.2015.05.002>.
- 1224 Baker, MA, Gibson, CH. 1987. Sampling turbulence in the stratified
1225 ocean: Statistical consequences of strong intermittency. *Journal of Phys-
1226 ical Oceanography* **17**(10): 1817–1836. doi:[https://doi.org/10.1175/1520-
1227 0485\(1987\)017<1817:STITSO>2.0.CO;2](https://doi.org/10.1175/1520-0485(1987)017<1817:STITSO>2.0.CO;2).
- 1228 Bates, N, Mathis, J. 2009. The Arctic Ocean marine carbon cycle: evaluation
1229 of air-sea CO₂ exchanges, ocean acidification impacts and potential feed-
1230 backs. *Biogeosciences* **6**(11): 2433–2459. doi:[https://doi.org/10.5194/bg-6-
1231 2433-2009](https://doi.org/10.5194/bg-6-2433-2009).
- 1232 Bates, NR, Moran, SB, Hansell, DA, Mathis, JT. 2006. An increasing CO₂ sink in
1233 the Arctic Ocean due to sea-ice loss. *Geophysical Research Letters* **33**(23).
1234 doi:<https://doi.org/10.1029/2006GL027028>.
- 1235 Bauch, D, Cherniavskaia, E, Timokhov, L. 2016. Shelf basin exchange along the
1236 Siberian continental margin: Modification of Atlantic Water and Lower Halo-
1237 cline Water. *Deep Sea Research Part I: Oceanographic Research Papers* **115**:
1238 188–198. doi:[10.1016/j.dsr.2016.06.008](https://doi.org/10.1016/j.dsr.2016.06.008).
- 1239 Bauch, D, van der Loeff, MR, Andersen, N, Torres-Valdes, S, Bakker, K, Abra-
1240 hamsen, EP. 2011. Origin of freshwater and polynya water in the Arctic
1241 Ocean halocline in summer 2007. *Progress in Oceanography* **91**(4): 482–
1242 495. doi:<https://doi.org/10.1016/j.pocean.2011.07.017>.
- 1243 Baumann, T, Fer, I, Bryhni, H, Peterson, AK, Allerholt, J, Fang, YC, Hoppmann,
1244 M, Karam, S, Koenig, Z, Kong, B, Mohrholz, V, Muilwijk, M, Schaffer, J,
1245 Schulz, K, Sukhikh, N, Tippenhauer, S. 2021. Under-ice current measure-
1246 ments during MOSAiC from a 75 kHz acoustic Doppler profiler. PANGAEA.
1247 doi:<https://doi.org/10.1594/PANGAEA.934792>.
- 1248 Bouffard, D, Boegman, L. 2013. A diapycnal diffusivity model for stratified en-
1249 vironmental flows. *Dynamics of Atmospheres and Oceans* **61**: 14–34. doi:
1250 <https://doi.org/10.1016/j.dynatmoce.2013.02.002>.
- 1251 Bourgain, P, Gascard, JC. 2011. The Arctic Ocean halocline and its interannual
1252 variability from 1997 to 2008. *Deep Sea Research Part I: Oceanographic Re-
1253 search Papers* **58**(7): 745–756. doi:<https://doi.org/10.1016/j.dsr.2011.05.001>.
- 1254 Boyd, TJ, Steele, M, Muench, RD, Gunn, JT. 2002. Partial recovery of the
1255 Arctic Ocean halocline. *Geophysical Research Letters* **29**(14): 2–1. doi:
1256 <https://doi.org/10.1029/2001GL014047>.

- 1257 Boyer, TP, Garcia, HE, Locarnini, RA, Zweng, MM, Mishonov, AV, Reagan,
1258 JR, Weathers, KA, Baranova, OK, Seidov, D, Smolyar, IV. 2018. World
1259 Ocean Atlas 2018. *NOAA National Centers for Environmental Information*
1260 <https://www.ncei.noaa.gov/archive/accession/NCEI-WOA18>.
- 1261 Carranza, MM, Gille, ST, Franks, PJ, Johnson, KS, Pinkel, R, Girton, JB.
1262 2018. When mixed layers are not mixed. Storm-driven mixing and
1263 bio-optical vertical gradients in mixed layers of the Southern Ocean.
1264 *Journal of Geophysical Research: Oceans* **123**(10): 7264–7289. doi:
1265 <https://doi.org/10.1029/2018JC014416>.
- 1266 Carter-Gates, M, Balestreri, C, Thorpe, SE, Cottier, F, Baylay, A, Bibby, TS,
1267 Moore, CM, Schroeder, DC. 2020. Implications of increasing Atlantic in-
1268 fluence for Arctic microbial community structure. *Scientific reports* **10**(1):
1269 19262. doi:<https://doi.org/10.1038/s41598-020-76293-x>.
- 1270 Charette, MA, Kipp, LE, Jensen, LT, Dabrowski, JS, Whitmore, LM, Fitzsim-
1271 mons, JN, Williford, T, Ulfso, A, Jones, E, Bundy, RM, Vivancos, SM,
1272 Pahnke, K, John, SG, Xiang, Y, Hatta, M, Petrova, MV, Heimbürger-
1273 Boavida, L, Bauch, D, Newton, R, Pasqualini, A, Agather, AM, Amon,
1274 RMW, Anderson, RF, Andersson, PS, Benner, R, Bowman, KL, Edwards,
1275 RL, Gdaniec, S, Gerringa, LJA, González, AG, Granskog, M, Haley, B,
1276 Hammerschmidt, CR, Hansell, DA, Henderson, PB, Kadko, DC, Kaiser, K,
1277 Laan, P, Lam, PJ, Lamborg, CH, Levier, M, Li, X, Margolin, AR, Mea-
1278 sures, C, Middag, R, Millero, FJ, Moore, WS, Paffrath, R, Planquette, H,
1279 Rabe, B, Reader, H, Rember, R, Rijkenberg, MJA, Roy-Barman, M, Rut-
1280 ters van der Loeff, M, Saito, M, Schauer, U, Schlosser, P, Sherrell, RM,
1281 Shiller, AM, Slagter, H, Sonke, JE, Stedmon, C, Woosley, RJ, Valk, O, Ooi-
1282 jen, J, Zhang, R. 2020. The Transpolar Drift as a source of riverine and
1283 shelf-derived trace elements to the central Arctic Ocean. *Journal of Geo-*
1284 *physical Research: Oceans* **125**(5): e2019JC015920. ISSN 2169-9275. doi:
1285 <https://doi.org/10.1029/2019JC015920>.
- 1286 Dossier, H, Chanona, M, Waterman, S, Shibley, N, Timmermans, ML. 2021.
1287 Changes in internal wave-driven mixing across the Arctic Ocean: Finescale
1288 estimates from an 18-year pan-Arctic record. *Geophysical Research Letters*
1289 **48**(8): e2020GL091747. doi:<https://doi.org/10.1029/2020GL091747>.
- 1290 Droste, ES, Hoppema, M, González-Dávila, M, Santana-Casiano, JM, Queste,
1291 BY, Dall’Olmo, G, Venables, HJ, Rohardt, G, Ossebaar, S, Schuller, D,
1292 Trace-Kleeberg, S, Bakker, DCE. 2022. The influence of tides on the ma-
1293 rine carbonate chemistry of a coastal polynya in the south-eastern Wed-
1294 dell Sea. *Ocean Science* **18**(5): 1293–1320. doi:<https://doi.org/10.5194/os->

- 1295 18-1293-2022.
- 1296 Erofeeva, S, Egbert, G. 2020. Arc5km2018: Arctic Ocean Inverse Tide
1297 Model on a 5 kilometer grid, 2018. Dataset. Arctic Data Center. doi:
1298 10.18739/A21R6N14K.
- 1299 Eveleth, R, Timmermans, ML, Cassar, N. 2014. Physical and biological controls
1300 on oxygen saturation variability in the upper Arctic Ocean. *Journal of Geo-*
1301 *physical Research: Oceans* **119**: 7420–7432. doi:10.1002/2014JC009816.
- 1302 Fer, I. 2009. Weak vertical diffusion allows maintenance of cold halocline in the
1303 central Arctic. *Atmospheric and Oceanic Science Letters* **2**(3): 148–152. doi:
1304 <https://doi.org/10.1080/16742834.2009.11446789>.
- 1305 Fer, I, Baumann, TM, Koenig, Z, Muilwijk, M, Tippenhauer, S. 2022.
1306 Upper-ocean turbulence structure and ocean-ice drag coefficient estimates
1307 using an ascending microstructure profiler during the MOSAiC drift.
1308 *Journal of Geophysical Research: Oceans* **127**(9): e2022JC018751. doi:
1309 <https://doi.org/10.1029/2022JC018751>.
- 1310 Fer, I, Müller, M, Peterson, A. 2015. Tidal forcing, energetics, and mixing near
1311 the Yermak Plateau. *Ocean Sci* **11**: 287–304. doi:[https://doi.org/10.5194/os-](https://doi.org/10.5194/os-11-287-2015)
1312 [11-287-2015](https://doi.org/10.5194/os-11-287-2015).
- 1313 Fine, EC, Cole, ST. 2022. Decadal observations of internal wave en-
1314 ergy, shear, and mixing in the western Arctic Ocean. *Journal*
1315 *of Geophysical Research: Oceans* **127**(5): e2021JC018056. doi:
1316 <https://doi.org/10.1029/2021JC018056>.
- 1317 Fong, AA, Hoppe, CJM, Aberle, N, Ashjian, CJ, Assmy, P, Bai, Y, Bakker, DCE,
1318 Balmonte, JP, Barry, KR, Bertilsson, S, Boulton, W, Bowman, J, Bozzato, D,
1319 Bratbak, G, Buck, M, Campbell, RG, Castellani, G, Chamberlain, EJ, Chen,
1320 J, Chierici, M, Cornils, A, Creamean, JM, Damm, E, Dethloff, K, Droste,
1321 ES, Ebenhöf, O, Eggers, SL, Engel, A, Flores, H, Fransson, A, Fricken-
1322 haus, S, Gardner, J, Gelfman, CE, Granskog, MA, Graeve, M, Havermans,
1323 C, Heuzé, C, Hildebrandt, N, Hill, TCJ, Hoppema, M, Immerz, A, Jin, H,
1324 Koch, B, Kong, X, Kraberg, A, Lan, M, Lange, BA, Larsen, A, Lebreton,
1325 B, Leu, E, Loose, B, Maslowski, W, Mavis, C, Metfies, K, Mock, T, Müller,
1326 O, Nicolaus, M, Niehoff, B, Nomura, D, Nöthig, EM, Oggier, M, Olden-
1327 burg, E, Olsen, LM, Peeken, I, Perovich, DK, Popa, O, Rabe, B, Ren, J, Rex,
1328 M, Rinke, A, Rokitta, S, Rost, B, Sakinan, S, Salganik, E, Schaafsma, FL,
1329 Schäfer, H, Schmidt, K, Shoemaker, KM, Shupe, MD, Snoeijs-Leijonmalm,
1330 P, Stefels, J, Svenson, A, Tao, R, Torres-Valdés, S, Torstensson, A, Tose-
1331 land, A, Ulfso, A, Van Leeuwe, MA, Vortkamp, M, Webb, AL, Gradinger,
1332 RR. 2023. Overview of the MOSAiC expedition: Ecosystem [preprint]. *Earth*

- 1333 *arXiv* doi:<https://doi.org/10.31223/X5P091>.
- 1334 Forget, G, Campin, JM, Heimbach, P, Hill, CN, Ponte, RM, Wunsch, C. 2015.
1335 ECCO version 4: An integrated framework for non-linear inverse mod-
1336 eling and global ocean state estimation. *Geoscientific Model Develop-*
1337 *ment* **8**(10): 3071–3104. ISSN 1991-9603. doi:[https://doi.org/10.5194/gmd-](https://doi.org/10.5194/gmd-8-3071-2015)
1338 [8-3071-2015](https://doi.org/10.5194/gmd-8-3071-2015).
- 1339 Fouest, VL, Babin, M, Tremblay, JÉ. 2013. The fate of riverine nutrients on Arctic
1340 shelves. *Biogeosciences* **10**(6): 3661–3677. doi:[https://doi.org/10.5194/bg-](https://doi.org/10.5194/bg-10-3661-2013)
1341 [10-3661-2013](https://doi.org/10.5194/bg-10-3661-2013).
- 1342 Fransson, A, Chierici, M, Skjelvan, I, Olsen, A, Assmy, P, Peterson, AK,
1343 Spreen, G, Ward, B. 2017. Effects of sea-ice and biogeochemical pro-
1344 cesses and storms on under-ice water fCO₂ during the winter-spring tran-
1345 sition in the high Arctic Ocean: Implications for sea-air CO₂ fluxes.
1346 *Journal of Geophysical Research: Oceans* **122**(7): 5566–5587. doi:
1347 <https://doi.org/10.1002/2016JC012478>.
- 1348 Friis, K, Körtzinger, A, Wallace, DW. 2003. The salinity normalization of marine
1349 inorganic carbon chemistry data. *Geophysical Research Letters* **30**(2). doi:
1350 <https://doi.org/10.1029/2002GL015898>.
- 1351 Galand, PE, Potvin, M, Casamayor, EO, Lovejoy, C. 2010. Hydrography shapes
1352 bacterial biogeography of the deep Arctic Ocean. *The ISME journal* **4**(4):
1353 564–576. doi:<https://doi.org/10.1038/ismej.2009.134>.
- 1354 Gibson, GA, Elliot, S, Clement Kinney, J, Piliouras, A, Jeffery, N.
1355 2022. Assessing the potential impact of river chemistry on arctic
1356 coastal production. *Frontiers in Marine Science* **9**: 738363. doi:
1357 <https://doi.org/10.3389/fmars.2022.738363>.
- 1358 Gonçalves-Araujo, R, Granskog, MA, Bracher, A, Azetsu-Scott, K, Dodd, PA,
1359 Stedmon, CA. 2016. Using fluorescent dissolved organic matter to trace and
1360 distinguish the origin of Arctic surface waters. *Scientific Reports* **6**(1): 33978.
1361 ISSN 2045-2322. doi:<https://doi.org/10.1038/srep33978>.
- 1362 Gonçalves-Araujo, R, Rabe, B, Peeken, I, Bracher, A. 2018. High colored dis-
1363 solved organic matter (CDOM) absorption in surface waters of the central-
1364 eastern Arctic Ocean: Implications for biogeochemistry and ocean color al-
1365 gorithms. *PLOS One* **13**: e0190838. doi:10.1371/journal.pone.0190838.
- 1366 Gordó-Vilaseca, C, Stephenson, F, Coll, M, Lavin, C, Costello, MJ. 2023. Three
1367 decades of increasing fish biodiversity across the northeast Atlantic and the
1368 Arctic Ocean. *Proceedings of the US National Academy of Sciences* **120**(4):
1369 e2120869120. doi:<https://doi.org/10.1073/pnas.2120869120>.
- 1370 Granskog, MA, Macdonald, RW, Mundy, CJ, Barber, DG. 2007. Distribution,

- 1371 characteristics and potential impacts of chromophoric dissolved organic mat-
1372 ter (CDOM) in Hudson Strait and Hudson Bay, Canada. *Continental Shelf*
1373 *Research* **27**: 2032–2050. doi:<https://doi.org/10.1016/j.csr.2007.05.001>.
- 1374 Granskog, MA, Pavlov, AK, Sagan, S, Kowalczyk, P, Raczkowska, A, Stedmon,
1375 CA. 2015. Effect of sea-ice melt on inherent optical properties and verti-
1376 cal distribution of solar radiant heating in Arctic surface waters. *Journal of*
1377 *Geophysical Research: Oceans* **120**(10): 7028–7039. ISSN 2169-9275. doi:
1378 10.1002/2015JC011087.
- 1379 Guthrie, J, Fer, I, Morison, J. 2017. Thermohaline staircases in the
1380 Amundsen Basin: possible disruption by shear and mixing. *Jour-*
1381 *nal of Geophysical Research: Oceans* **122**: 7767– 7782. doi:
1382 <https://doi.org/10.1002/2017JC012993>.
- 1383 Haas, C, Hoppmann, M, Tippenhauer, S, Rohardt, G. 2021. Continuous thermos-
1384 alinograph oceanography along RV POLARSTERN cruise track PS122/2.
1385 PANGAEA. doi:<https://doi.org/10.1594/PANGAEA.930024>.
- 1386 Han, D, Ha, HK, Hwang, CY, Lee, BY, Hur, HG, Lee, YK. 2015. Bacterial
1387 communities along stratified water columns at the Chukchi Borderland in
1388 the western Arctic Ocean. *Deep Sea Research Part II: Topical Studies in*
1389 *Oceanography* **120**: 52–60. doi:<https://doi.org/10.1016/j.dsr2.2015.01.018>.
- 1390 Heuzé, C, Huhn, O, Walter, M, Sukhikh, N, Karam, S, Körtke, W, Vredenburg, M,
1391 Bulsiewicz, K, Sültenfuß, J, Fang, YC, Mertens, C, Rabe, B, Tippenhauer, S,
1392 Allerholt, J, He, H, Kuhlmeier, D, Kuznetsov, I, Mallet, M. 2023a. A year of
1393 transient tracers chlorofluorocarbon 12 and sulfur hexafluoride, noble gases
1394 helium and neon, and tritium in the Arctic Ocean from the MOSAiC expedi-
1395 tion (2019-2020). *Earth System Science Data Discussions* doi:10.5194/essd-
1396 2023-232.
- 1397 Heuzé, C, Zanowski, H, Karam, S, Muilwijk, M. 2023b. The deep Arctic Ocean
1398 and Fram Strait in CMIP6 models. *Journal of Climate* **36**(8): 2551–2584.
1399 doi:<https://doi.org/10.1175/JCLI-D-22-0194.1>.
- 1400 Hill, VJ. 2008. Impacts of chromophoric dissolved organic material on surface
1401 ocean heating in the Chukchi Sea. *Journal of Geophysical Research* **113**:
1402 C07024. doi:10.1029/2007JC004119.
- 1403 Hoppmann, M, Kuznetsov, I, Fang, YC, Rabe, B. 2022. Processed data of CTD
1404 buoys 2019O1 to 2019O8 as part of the MOSAiC Distributed Network. PAN-
1405 GAEA. doi:<https://doi.org/10.1594/PANGAEA.940320>.
- 1406 Jakobsson, M, Mayer, LA, Bringensparr, C, Castro, CF, Mohammad, R, John-
1407 son, P, Ketter, T, Accettella, D, Amblas, D, An, L, Arndt, JE, Canals, M,
1408 Casamor, JL, Chauché, N, Coakley, B, Danielson, S, Demarte, M, Dickson,

- 1409 ML, Dorschel, B, Dowdeswell, JA, Dreutter, S, Fremand, AC, Gallant, D,
 1410 Hall, JK, Hehemann, L, Hodnesdal, H, Hong, J, Ivaldi, R, Kane, E, Klaucke,
 1411 I, Krawczyk, DW, Kristoffersen, Y, Kuipers, BR, Millan, R, Masetti, G,
 1412 Morlighem, M, Noormets, R, Prescott, MM, Rebesco, M, Rignot, E, Semile-
 1413 tov, I, Tate, AJ, Travaglini, P, Velicogna, I, Weatherall, P, Weinrebe, W,
 1414 Willis, JK, Wood, M, Zarayskaya, Y, Zhang, T, Zimmermann, M, Zinglensen,
 1415 KB. 2020. The international bathymetric chart of the Arctic Ocean version
 1416 4.0. *Scientific data* **7**(1): 176. doi:[https://doi.org/10.1038/s41597-020-0520-](https://doi.org/10.1038/s41597-020-0520-9)
 1417 [9](https://doi.org/10.1038/s41597-020-0520-9).
- 1418 Janout, MA, Hölemann, J, Laukert, G, Smirnov, A, Krumpfen, T, Bauch, D,
 1419 Timokhov, L. 2020. On the variability of stratification in the freshwater-
 1420 influenced Laptev Sea Region. *Frontiers in Marine Science* **7**: 543489. doi:
 1421 <https://doi.org/10.3389/fmars.2020.543489>.
- 1422 Juranek, LW. 2022. Changing biogeochemistry of the Arctic Ocean. *Oceanogra-*
 1423 *phy* **35**(3/4): 144–155. doi:<https://doi.org/10.5670/oceanog.2022.120>.
- 1424 Kanzow, T, Hoppmann, M, Tippenhauer, S, Rohardt, G. 2021. Continuous
 1425 thermosalinograph oceanography along RV POLARSTERN cruise track
 1426 PS122/3. PANGAEA. doi:<https://doi.org/10.1594/PANGAEA.930026>.
- 1427 Karam, S, Heuzé, C, Hoppmann, M, de Steur, L. 2024. Con-
 1428 tinued warming of deep waters in Fram Strait. *EGU-*
 1429 *sphere* **2024**: 1–23. doi:10.5194/egusphere-2024-458.
 1430 <https://egusphere.copernicus.org/preprints/2024/egusphere-2024-458/>.
- 1431 Karam, S, Heuzé, C, Müller, V, Zheng, Y. 2023. Recirculation of Canada
 1432 Basin Deep Water in the Amundsen Basin, Arctic. *Journal of Physi-*
 1433 *cal Oceanography* **53**(11): 2559 – 2574. doi:10.1175/JPO-D-22-0252.1.
 1434 <https://journals.ametsoc.org/view/journals/phoc/53/11/JPO-D-22-0252.1>.
- 1435 Karcher, M, Smith, JN, Kauker, F, Gerdes, R, Smethie, WM. 2012. Re-
 1436 cent changes in Arctic Ocean circulation revealed by iodine-129 observa-
 1437 tions and modeling. *Journal of Geophysical Research* **117**: C08007. doi:
 1438 [10.1029/2011JC007513](https://doi.org/10.1029/2011JC007513).
- 1439 Kawaguchi, Y, Koenig, Z, Nomura, D, Hoppmann, M, Inoue, J, Fang, YC,
 1440 Schulz, K, Gallagher, M, Katlein, C, Nicolaus, M, Rabe, B. 2022.
 1441 Turbulent mixing during late summer in the ice–ocean boundary layer
 1442 in the central Arctic Ocean: Results from the MOSAiC expedition.
 1443 *Journal of Geophysical Research: Oceans* **127**(8): e2021JC017975. doi:
 1444 <https://doi.org/10.1029/2021JC017975>.
- 1445 Kim, YH, Min, SK, Gillett, NP, Notz, D, Malinina, E. 2023. Observationally-
 1446 constrained projections of an ice-free Arctic even under a low emission sce-

- 1447 nario. *Nature Communications* **14**. doi:[https://doi.org/10.1038/s41467-023-](https://doi.org/10.1038/s41467-023-38511-8)
1448 38511-8.
- 1449 Knust, R. 2017. Polar research and supply vessel POLARSTERN operated by
1450 the Alfred-Wegener-Institute. *Journal of Large-Scale Research Facilities* **3**:
1451 A119. doi:<https://doi.org/10.17815/jlsrf-3-163>.
- 1452 Kong, X. 2022. *Molecular and optical characterization of dissolved*
1453 *organic matter in the Central Arctic Ocean*. Phd thesis, Uni-
1454 versity of Bremen, Dissertation, 2022, Bremen. 159 pages.
1455 <https://suche.suub.uni-bremen.de/peid=B183177399>.
- 1456 Korhonen, M, Rudels, B, Marnela, M, Wisotzki, A, Zhao, J. 2013. Time and
1457 space variability of freshwater content, heat content and seasonal ice melt
1458 in the Arctic Ocean from 1991 to 2011. *Ocean Science* **9**(6): 1015–1055.
1459 doi:<https://doi.org/10.5194/osd-9-2621-2012>.
- 1460 Krishfield, R, Toole, J, Proshutinsky, A, Timmermans, ML. 2008. Automated ice-
1461 tethered profilers for seawater observations under pack ice in all seasons.
1462 *Journal of Atmospheric and Oceanic Technology* **25**(11): 2091–2105. doi:
1463 <https://doi.org/10.1175/2008JTECHO587.1>.
- 1464 Krumpfen, T, Belter, HJ, Boetius, A, Damm, E, Haas, C, Hendricks, S, Nico-
1465 laus, M, Nöthig, EM, Paul, S, Peeken, I, Ricker, R, Stein, R. 2019. Arc-
1466 tic warming interrupts the Transpolar Drift and affects long-range trans-
1467 port of sea ice and ice-rafted matter. *Scientific Reports* **9**(1): 5459. doi:
1468 <https://doi.org/10.1038/s41598-019-41456-y>.
- 1469 Kwok, R. 2018. Arctic sea ice thickness, volume, and multiyear ice coverage:
1470 losses and coupled variability (1958–2018). *Environmental Research Letters*
1471 **13**(10): 105005. doi:<https://doi.org/10.1088/1748-9326/aae3ec>.
- 1472 Lannuzel, D, Tedesco, L, Van Leeuwe, M, Campbell, K, Flores, H, Delille, B,
1473 Miller, L, Stefels, J, Assmy, P, Bowman, J, Brown, K, Castellani, G, Chierici,
1474 M, Crabeck, O, Damm, E, Else, B, Fransson, A, Fripiat, F, Geilfus, NX,
1475 Jacques, C, Jones, E, Kaartokallio, H, Kotovitch, M, Meiners, K, Moreau, S,
1476 Nomura, D, Peeken, I, Rintala, JM, Steiner, N, Tison, JL, Vancoppenolle, M,
1477 Van der Linden, F, Vichi, M, Wongpan, P. 2020. The future of Arctic sea-
1478 ice biogeochemistry and ice-associated ecosystems. *Nature Climate Change*
1479 **10**(11): 983–992. doi:<https://doi.org/10.1038/s41558-020-00940-4>.
- 1480 Laukert, G, Frank, M, Bauch, D, Hathorne, EC, Rabe, B, von Appen, WJ, Weg-
1481 ner, C, Zieringer, M, Kassens, H. 2017. Ocean circulation and freshwater
1482 pathways in the Arctic Mediterranean based on a combined Nd isotope, REE
1483 and oxygen isotope section across Fram Strait. *Geochimica et Cosmochimica*
1484 *Acta* **202**: 285–309. doi:<https://doi.org/10.1016/j.gca.2016.12.028>.

- 1485 Laukert, G, Grasse, P, Novikhin, A, Povazhnyi, V, Doering, K, Hölemann, J,
1486 Janout, M, Bauch, D, Kassens, H, Frank, M. 2022. Nutrient and silicon iso-
1487 tope dynamics in the Laptev Sea and implications for nutrient availability in
1488 the transpolar drift. *Global Biogeochemical Cycles* **36**(9): e2022GB007316.
1489 doi:<https://doi.org/10.1029/2022GB007316>.
- 1490 Laukert, G, Makhotin, M, Petrova, MV, Frank, M, Hathorne, EC, Bauch,
1491 D, Böning, P, Kassens, H. 2019. Water mass transformation in the Bar-
1492 ents Sea inferred from radiogenic neodymium isotopes, rare earth ele-
1493 ments and stable oxygen isotopes. *Chemical Geology* **511**: 416–430. doi:
1494 <https://doi.org/10.1016/j.chemgeo.2018.10.002>.
- 1495 Lei, R, Cheng, B, Hoppmann, M, Zhang, F, Zuo, G, Hutchings, JK, Lin,
1496 L, Lan, M, Wang, H, Regnery, J, Krumpfen, T, Haapala, J, Rabe,
1497 B, Perovich, DK, Nicolaus, M. 2022. Seasonality and timing of sea
1498 ice mass balance and heat fluxes in the Arctic transpolar drift during
1499 2019–2020. *Elementa Science of the Anthropocene* **10**(1): 000089. doi:
1500 <https://doi.org/10.1525/elementa.2021.000089>.
- 1501 Lenn, YD, Wiles, P, Torres-Valdes, S, Abrahamsen, E, Rippeth, T, Simpson, J,
1502 Bacon, S, Laxon, S, Polyakov, I, Ivanov, V, Kirillov, S. 2009. Vertical mixing
1503 at intermediate depths in the Arctic boundary current. *Geophysical Research*
1504 *Letters* **36**(5). doi:<https://doi.org/10.1029/2008GL036792>.
- 1505 Li, WK, McLaughlin, FA, Lovejoy, C, Carmack, EC. 2009. Smallest algae
1506 thrive as the Arctic Ocean freshens. *Science* **326**(5952): 539–539. doi:
1507 [10.1126/science.1179798](https://doi.org/10.1126/science.1179798).
- 1508 Llanillo, P, Aiken, CM, Cordero, R, Damiani, A, Sepúlveda, E, Fernández-
1509 Gómez, B. 2019. Oceanographic variability induced by tides, the in-
1510 traseasonal cycle and warm subsurface water intrusions in Maxwell Bay,
1511 King George Island (West-Antarctica). *Scientific reports* **9**(1): 18571. doi:
1512 <https://doi.org/10.1038/s41598-019-54875-8>.
- 1513 Locarnini, R, Mishonov, A, Baranova, O, Boyer, T, Zweng, M, Garcia, H, Rea-
1514 gan, J, Seidov, D, Weathers, K, Paver, C, Smolyar, I. 2018. *World Ocean At-*
1515 *las 2018, Volume 1: Temperature*. A. Mishonov Technical Ed.; NOAA Atlas
1516 NESDIS 81.
- 1517 Marnela, M, Rudels, B, Goszczko, I, Beszczynska-Möller, A, Schauer, U. 2016.
1518 Fram Strait and Greenland Sea transports, water masses, and water mass
1519 transformations 1999–2010 (and beyond). *Journal of Geophysical Research:*
1520 *Oceans* **121**(4): 2314–2346. doi:<https://doi.org/10.1002/2015JC011312>.
- 1521 McDougall, TJ, Barker, PM. 2011. Getting started with TEOS-10 and the Gibbs
1522 Seawater (GSW) oceanographic toolbox. *SCOR/IAPSO WG* **127**: 1–28.

- 1523 McPhee, M. 2008. *Air-ice-ocean interaction: Turbulent ocean boundary layer ex-*
1524 *change processes*. Springer Science & Business Media.
- 1525 Meyer, A, Fer, I, Sundfjord, A, Peterson, AK. 2017a. Mixing rates and
1526 vertical heat fluxes north of Svalbard from Arctic winter to spring.
1527 *Journal of Geophysical Research: Oceans* **122**(6): 4569–4586. doi:
1528 <https://doi.org/10.1002/2016JC012441>.
- 1529 Meyer, A, Sundfjord, A, Fer, I, Provost, C, Villaciers Robineau, N,
1530 Koenig, Z, Onarheim, IH, Smedsrud, LH, Duarte, P, Dodd, PA, Gra-
1531 ham, RM, Schmidtko, S, Kauko, HM. 2017b. Winter to summer
1532 oceanographic observations in the Arctic Ocean north of Svalbard.
1533 *Journal of Geophysical Research: Oceans* **122**(8): 6218–6237. doi:
1534 <https://doi.org/10.1002/2016JC012391>.
- 1535 Mieruch, S. 2023. smieruch/mosaic_hydrographic_core_parameters:
1536 Initial Release. Zenodo. doi:10.5281/zenodo.8304184.
1537 <https://doi.org/10.5281/zenodo.8304184>.
- 1538 Mieruch, S, Schlitzer, R. 2023. smieruch/webodv: we-
1539 bodv v1.0.0. Zenodo. doi:10.5281/zenodo.8241241.
1540 <https://doi.org/10.5281/zenodo.8241241>.
- 1541 Morán, XAG, López-Urrutia, Á, Calvo-Díaz, A, Li, WK. 2010. Increasing im-
1542 portance of small phytoplankton in a warmer ocean. *Global Change Biology*
1543 **16**(3): 1137–1144. doi:<https://doi.org/10.1111/j.1365-2486.2009.01960.x>.
- 1544 Mysak, LA. 2001. Patterns of Arctic Circulation. *Science* **293**(5533): 1269–1270.
1545 doi:DOI: 10.1126/science.1064217.
- 1546 Nguyen, AT, Pillar, H, Ocaña, V, Bigdeli, A, Smith, TA, Heimbach, P. 2021. The
1547 Arctic Subpolar Gyre sTate Estimate: Description and assessment of a data-
1548 constrained, dynamically consistent ocean-sea ice estimate for 2002–2017.
1549 *Journal of Advances in Modeling Earth Systems* **13**(5): e2020MS002398.
1550 doi:<https://doi.org/10.1029/2020MS002398>.
- 1551 Nicolaus, M, Perovich, DK, Spreen, G, Granskog, MA, von Albedyll, L, An-
1552 gelopoulos, M, Anhaus, P, Arndt, S, Belter, HJ, Bessonov, V, Birnbaum,
1553 G, Brauchle, J, Calmer, R, Cardellach, E, Cheng, B, Clemens-Sewall, D,
1554 Dadic, R, Damm, E, de Boer, G, Demir, O, Dethloff, K, Divine, DV, Fong,
1555 AA, Fons, S, Frey, MM, Fuchs, N, Gabarró, C, Gerland, S, Goessling, HF,
1556 Gradinger, R, Haapala, J, Haas, C, Hamilton, J, Hannula, HR, Hendricks, S,
1557 Herber, A, Heuzé, C, Hoppmann, M, Høyland, KV, Huntemann, M, Hutch-
1558 ings, JK, Hwang, B, Itkin, P, Jacobi, HW, Jaggi, M, Jutila, A, Kaleschke, L,
1559 Katlein, C, Kolabutin, N, Krampe, D, Kristensen, SS, Krumpfen, T, Kurtz, N,
1560 Lampert, A, Lange, BA, Lei, R, Light, B, Linhardt, F, Liston, GE, Loose,

- 1561 B, Macfarlane, AR, Mahmud, M, Matero, IO, Maus, S, Morgenstern, A,
1562 Naderpour, R, Nandan, V, Niubom, A, Oggier, M, Oppelt, N, Pätzold, F,
1563 Perron, C, Petrovsky, T, Pirazzini, R, Polashenski, C, Rabe, B, Raphael, IA,
1564 Regnery, J, Rex, M, Ricker, R, Riemann-Campe, K, Rinke, A, Rohde, J,
1565 Salganik, E, Scharien, RK, Schiller, M, Schneebeil, M, Semmling, M, Shi-
1566 manchuk, E, Shupe, MD, Smith, MM, Smolyanitsky, V, Sokolov, V, Stanton,
1567 T, Stroeve, J, Thielke, L, Timofeeva, A, Tonboe, RT, Tavri, A, Tsamados,
1568 M, Wagner, DN, Watkins, D, Webster, M, Wendisch, M. 2022. Overview of
1569 the MOSAiC expedition: Snow and sea ice. *Elem Sci Anth* **10**(1): 000046.
1570 doi:<https://doi.org/10.1525/elementa.2021.000046>.
- 1571 Nicolaus, M, Riemann-Campe, K, Bliss, A, Hutchings, JK, Granskog,
1572 MA, Haas, C, Hoppmann, M, Kanzow, T, Krishfield, RA, Lei, R,
1573 Rex, M, Li, T, Rabe, B. 2021. Drift trajectories of the main sites
1574 of the Distributed Network of MOSAiC 2019/2020. PANGAEA. doi:
1575 <https://doi.org/10.1594/PANGAEA.937204>.
- 1576 Nixdorf, U, Dethloff, K, Rex, M, Shupe, M, Sommerfeld, A, Perovich, DK,
1577 Nicolaus, M, Heuzé, C, Rabe, B, Loose, B, Damm, E, Gradinger, R, Fong,
1578 A, Maslowski, W, Rinke, A, Kwok, R, Spreen, G, Wendisch, M, Her-
1579 ber, A, Hirsekorn, M, Mohaupt, V, Frickenhaus, S, Immerz, A, Weiss-
1580 Tuider, K, König, B, Mengedoht, D, Regnery, J, Gerchow, P, Ransby, D,
1581 Krumpfen, T, Morgenstern, A, Haas, C, Kanzow, T, Rack, FR, Saitzev,
1582 V, Sokolov, V, Makarov, A, Schwarze, S, Wunderlich, T, Wurr, K,
1583 Boetius, A. 2021. MOSAiC Extended Acknowledgement. Zenodo. doi:
1584 <https://doi.org/10.5281/zenodo.5541624>.
- 1585 Nomura, D, Kawaguchi, Y, Webb, AL, Li, Y, Dall'osto, M, Schmidt, K,
1586 Droste, ES, Chamberlain, EJ, Kolabutin, N, Shimanchuk, E, Hoppmann,
1587 M, Gallagher, MR, Meyer, H, Mellat, M, Bauch, D, Gabarró, C, Smith,
1588 MM, Inoue, J, Damm, E, Delille, B. 2023. Meltwater layer dynamics
1589 in a central Arctic lead: Effects of lead width, re-freezing, and mixing
1590 during late summer. *Elementa: Science of the Anthropocene* **11**(1). doi:
1591 <https://doi.org/10.1525/elementa.2022.00102>.
- 1592 Paffrath, R, Laukert, G, Bauch, D, Rutgers van der Loeff, M, Pahnke, K.
1593 2021. Separating individual contributions of major Siberian rivers in the
1594 Transpolar Drift of the Arctic Ocean. *Scientific Reports* **11**(1): 1–11. doi:
1595 <https://doi.org/10.1038/s41598-021-86948-y>.
- 1596 Pavlov, AK, Granskog, MA, Stedmon, CA, Ivanov, BV, Hudson, SR, Falk-
1597 Petersen, S. 2015. Contrasting optical properties of surface waters across the
1598 Fram Strait and its potential biological implications. *Journal of Marine Sys-*

- 1599 *tems* **143**: 62–72. ISSN 09247963. doi:10.1016/j.jmarsys.2014.11.001.
- 1600 Peralta-Ferriz, C, Woodgate, RA. 2015. Seasonal and interannual variability
1601 of pan-Arctic surface mixed layer properties from 1979 to 2012
1602 from hydrographic data, and the dominance of stratification for multiyear
1603 mixed layer depth shoaling. *Progress in Oceanography* **134**: 19–53. doi:
1604 <https://doi.org/10.1016/j.pocean.2014.12.005>.
- 1605 Perovich, D, Raphael, I, Moore, R, Clemens-Sewall, D, Lei, R, Sledd, A, Po-
1606 lashenski, C. 2023. Sea ice heat and mass balance measurements from four
1607 autonomous buoys during the MOSAiC drift campaign. *Elementa: Science of*
1608 *the Anthropocene* **11**(1). doi:<https://doi.org/10.1525/elementa.2023.00017>.
- 1609 Polyakov, IV, Ingvaldsen, RB, Pnyushkov, AV, Bhatt, US, Francis, JA, Janout, M,
1610 Kwok, R, Skagseth, Ø. 2023. Fluctuating Atlantic inflows modulate Arctic
1611 atlantification. *Science* **381**(6661): 972–979. doi:10.1126/science.adh5158.
- 1612 Polyakov, IV, Pnyushkov, AV, Alkire, MB, Ashik, IM, Baumann, TM, Carmack,
1613 EC, Goszczko, I, Guthrie, J, Ivanov, VV, Kanzow, T, Krishfield, R, Kwok,
1614 R, Sundfjord, A, Morison, J, Rember, R, Yulin, A. 2017. Greater role for
1615 Atlantic inflows on sea-ice loss in the Eurasian Basin of the Arctic Ocean.
1616 *Science* **356**(6335): 285–291. doi:<https://doi.org/10.1126/science.aai8204>.
- 1617 Polyakov, IV, Rippeth, TP, Fer, I, Alkire, MB, Baumann, TM, Carmack, EC, Ing-
1618 valdsen, R, Ivanov, VV, Janout, M, Lind, S, Padman, L, Pnyushkov, AV, Rem-
1619 ber, R. 2020a. Weakening of cold halocline layer exposes sea ice to oceanic
1620 heat in the eastern Arctic Ocean. *Journal of Climate* **33**(18): 8107–8123. doi:
1621 <https://doi.org/10.1175/JCLI-D-19-0976.1>.
- 1622 Polyakov, IV, Rippeth, TP, Fer, I, Baumann, TM, Carmack, EC, Ivanov,
1623 VV, Janout, M, Padman, L, Pnyushkov, AV, Rember, R. 2020b. In-
1624 tensification of near-surface currents and shear in the Eastern Arc-
1625 tic Ocean. *Geophysical Research Letters* **47**(16): e2020GL089469. doi:
1626 <https://doi.org/10.1029/2020GL089469>.
- 1627 Priest, T, von Appen, WJ, Oldenburg, E, Popa, O, Torres-Valdés, S, Bienhold,
1628 C, Metfies, K, Boulton, W, Mock, T, Fuchs, BM, Amann, R, Boetius, A,
1629 Wietz, M. 2023. Atlantic water influx and sea-ice cover drive taxonomic and
1630 functional shifts in Arctic marine bacterial communities. *The ISME Journal*
1631 pp. 1–14. doi:<https://doi.org/10.1038/s41396-023-01461-6>.
- 1632 Rabe, B, Heuzé, C, Regnery, J, Aksenov, Y, Allerholt, J, Athanase, M, Bai, Y,
1633 Basque, C, Bauch, D, Baumann, TM, Chen, D, Cole, ST, Craw, L, Davies,
1634 A, Damm, E, Dethloff, K, Divine, DV, Doglioni, F, Ebert, F, Fang, YC, Fer, I,
1635 Fong, AA, Gradinger, R, Granskog, MA, Graupner, R, Haas, C, He, H, He, Y,
1636 Hoppmann, M, Janout, M, Kadko, D, Kanzow, T, Karam, S, Kawaguchi, Y,

- 1637 Koenig, Z, Kong, B, Krishfield, RA, Krumpfen, T, Kuhlmeier, D, Kuznetsov, I,
1638 Lan, M, Lei, R, Li, T, Torres-Valdés, S, Lin, L, Lin, L, Liu, H, Liu, N, Loose,
1639 B, Ma, X, MacKay, R, Mallet, M, Mallett, RDC, Maslowski, W, Mertens,
1640 C, Mohrholz, V, Muilwijk, M, Nicolaus, M, O'Brien, JK, Perovich, D, Ren,
1641 J, Rex, M, Ribeiro, N, Rinke, A, Schaffer, J, Schuffenhauer, I, Schulz, K,
1642 Shupe, MD, Shaw, W, Sokolov, V, Sommerfeld, A, Spreen, G, Stanton, T,
1643 Stephens, M, Su, J, Sukhikh, N, Sundfjord, A, Thomisch, K, Tippenhauer,
1644 S, Toole, JM, Vredenburg, M, Walter, M, Wang, H, Wang, L, Wang, Y,
1645 Wendisch, M, Zhao, J, Zhou, M, Zhu, J, Laukert, G. 2022. Overview of the
1646 MOSAiC expedition: Physical oceanography. *Elementa: Science of the An-*
1647 *thropocene* **10**(1). doi:<https://doi.org/10.1525/elementa.2021.00062>.
- 1648 Randelhoff, A, Holding, J, Janout, M, Sejr, MK, Babin, M, Tremblay, JE,
1649 Alkire, MB. 2020. Pan-Arctic ocean primary production constrained
1650 by turbulent nitrate fluxes. *Frontiers in Marine Science* **7**: 150. doi:
1651 <https://doi.org/10.3389/fmars.2020.00150>.
- 1652 Rantanen, M, Karpechko, AY, Lipponen, A, Nordling, K, Hyvärinen, O, Ruos-
1653 teenoja, K, Vihma, T, Laaksonen, A. 2022. The Arctic has warmed nearly
1654 four times faster than the globe since 1979. *Communications Earth & Envi-*
1655 *ronment* **3**(1): 168. doi:<https://doi.org/10.1038/s43247-022-00498-3>.
- 1656 Rex, M, Hoppmann, M, Tippenhauer, S, Rohardt, G. 2021a. Continuous thermos-
1657 alinograph oceanography along RV POLARSTERN cruise track PS122/1.
1658 PANGAEA. doi:<https://doi.org/10.1594/PANGAEA.930023>.
- 1659 Rex, M, Hoppmann, M, Tippenhauer, S, Rohardt, G. 2021b. Continuous thermos-
1660 alinograph oceanography along RV POLARSTERN cruise track PS122/4.
1661 PANGAEA. doi:<https://doi.org/10.1594/PANGAEA.930027>.
- 1662 Rex, M, Hoppmann, M, Tippenhauer, S, Rohardt, G. 2021c. Continuous thermos-
1663 alinograph oceanography along RV POLARSTERN cruise track PS122/5.
1664 PANGAEA. doi:<https://doi.org/10.1594/PANGAEA.930028>.
- 1665 Rippeth, TP, Lincoln, BJ, Lenn, YD, Green, JM, Sundfjord, A, Ba-
1666 con, S. 2015. Tide-mediated warming of Arctic halocline by Atlantic
1667 heat fluxes over rough topography. *Nature Geoscience* **8**(3): 191. doi:
1668 <https://doi.org/10.1038/ngeo2350>.
- 1669 Rogge, A, Janout, M, Loginova, N, Trudnowska, E, Hörstmann, C, Wekerle, C,
1670 Oziel, L, Schourup-Kristensen, V, Ruiz-Castillo, E, Schulz, K, Povazhnyy,
1671 VV, Iversen, MH, Waite, AM. 2023. Carbon dioxide sink in the Arctic Ocean
1672 from cross-shelf transport of dense Barents Sea water. *Nature Geoscience*
1673 **16**(1): 82–88. doi:<https://doi.org/10.1038/s41561-022-01069-z>.
- 1674 Rudels, B. 2009. Arctic Ocean Circulation. Academic Press.

- 1675 Rudels, B. 2012. Arctic Ocean circulation and variability-advection and exter-
1676 nal forcing encounter constraints and local processes. *Ocean Science* doi:
1677 <https://doi.org/10.5194/os-8-261-2012>.
- 1678 Rudels, B. 2015. Arctic Ocean circulation, processes and water masses: A de-
1679 scription of observations and ideas with focus on the period prior to the In-
1680 ternational Polar Year 2007–2009. *Progress in Oceanography* **132**: 22–67.
1681 doi:<https://doi.org/10.1016/j.pocean.2013.11.006>.
- 1682 Rudels, B, Hainbucher, D. 2020. On the formation and spreading of thermohaline
1683 intrusions in the Arctic Ocean. *Geophysica* **55**(1-2): 23–59.
- 1684 Salganik, E, Katlein, C, Lange, BA, Matero, I, Lei, R, Fong, AA, Fons, SW, Di-
1685 vine, D, Oggier, M, Castellani, G, Bozzato, D, Chamberlain, EJ, Hoppe,
1686 CJM, Müller, O, Gardner, J, Rinke, A, Pereira, PS, Ulfsbo, A, Marsay, C,
1687 Webster, MA, Maus, S, Høyland, KV, Granskog, MA. 2023a. Temporal evo-
1688 lution of under-ice meltwater layers and false bottoms and their impact on
1689 summer Arctic sea ice mass balance. *Elementa: Science of the Anthropocene*
1690 **11**(1). doi:<https://doi.org/10.1525/elementa.2022.00035>.
- 1691 Salganik, E, Lange, BA, Katlein, C, Matero, I, Anhaus, P, Muilwijk, M, Høyland,
1692 KV, Granskog, MA. 2023b. Observations of preferential summer melt of
1693 Arctic sea-ice ridge keels from repeated multibeam sonar surveys. *The*
1694 *Cryosphere* **17**(11): 4873–4887. doi:10.5194/tc-17-4873-2023.
- 1695 Schauer, U, Muench, RD, Rudels, B, Timokhov, L. 1997. Impact of east-
1696 ern Arctic shelf waters on the Nansen Basin intermediate layers.
1697 *Journal of Geophysical Research: Oceans* **102**(C2): 3371–3382. doi:
1698 <https://doi.org/10.1029/96JC03366>.
- 1699 Schmale, J, Zieger, P, Ekman, AM. 2021. Aerosols in current and fu-
1700 ture Arctic climate. *Nature Climate Change* **11**(2): 95–105. doi:
1701 <https://doi.org/10.1038/s41558-020-00969-5>.
- 1702 Schmidtko, S, Johnson, GC, Lyman, JM. 2013. MIMOC: A global
1703 monthly isopycnal upper-ocean climatology with mixed layers. *Jour-
1704 nal of Geophysical Research: Oceans* **118**(4). ISSN 21699291. doi:
1705 <https://doi.org/10.1002/jgrc.20122>.
- 1706 Schulz, K, Janout, M, Lenn, YD, Ruiz-Castillo, E, Polyakov, I, Mohrholz, V,
1707 Tippenhauer, S, Reeve, K, Hölemann, J, Rabe, B, Vredenburg, M. 2021.
1708 On the along-slope heat loss of the Boundary Current in the Eastern Arctic
1709 Ocean. *Journal of Geophysical Research: Oceans* **126**(2): e2020JC016375.
1710 doi:<https://doi.org/10.1029/2020JC016375>.
- 1711 Schulz, K, Kadko, D, Mohrholz, V, Stephens, M, Fer, I. 2023a. Winter verti-
1712 cal diffusion rates in the Arctic Ocean, estimated from ⁷Be measurements

- 1713 and dissipation rate profiles. *Journal of Geophysical Research: Oceans* pp.
1714 e2022JC019197. doi:<https://doi.org/10.1029/2022JC019197>.
- 1715 Schulz, K, Koenig, Z, Muilwijk, M. 2023b. The Eurasian Arctic Ocean along
1716 the MOSAiC drift (2019-2020): Core hydrographic parameters. Arctic Data
1717 Center. doi:[doi:10.18739/A21J9790B](https://doi.org/10.18739/A21J9790B).
- 1718 Schulz, K, Lincoln, B, Povazhnyy, V, Rippeth, T, Lenn, YD, Janout, M, Alkire, M,
1719 Scannell, B, Torres-Valdés, S. 2022a. Increasing nutrient fluxes and mixing
1720 regime changes in the eastern Arctic Ocean. *Geophysical Research Letters*
1721 pp. e2021GL096152. doi:<https://doi.org/10.1029/2021GL096152>.
- 1722 Schulz, K, Mohrholz, V, Fer, I, Janout, M, Hoppmann, M, Schaffer, J, Koenig,
1723 Z. 2022b. A full year of turbulence measurements from a drift cam-
1724 paign in the Arctic Ocean 2019—2020. *Scientific Data* **9**(472). doi:
1725 <https://doi.org/10.1038/s41597-022-01574-1>.
- 1726 Schulz, K, Mohrholz, V, Fer, I, Janout, MA, Hoppmann, M, Schaffer, J, Koenig,
1727 Z, Rabe, B, Heuzé, C, Regnery, J, Allerholt, J, Fang, YC, He, H, Kanzow,
1728 T, Karam, S, Kuznetsov, I, Kong, B, Liu, H, Muilwijk, M, Schuffenhauer, I,
1729 Sukhikh, N, Sundfjord, A, Tippenhauer, S. 2023c. Turbulent microstructure
1730 profile (MSS) measurements from the MOSAiC drift, Arctic Ocean, version
1731 2. PANGAEA. doi:<https://doi.pangaea.de/10.1594/PANGAEA.961798>.
- 1732 Schuster, U, McKinley, GA, Bates, N, Chevallier, F, Doney, SC, Fay, AR,
1733 González-Dávila, M, Gruber, N, Jones, S, Krijnen, J, Landschützer, P,
1734 Lefèvre, N, Manizza, M, Mathis, J, Metzl, N, Olsen, A, Rios, AF, Rödenbeck,
1735 C, Santana-Casiano, JM, Takahashi, T, Wanninkhof, R, Watson, AJ. 2013. An
1736 assessment of the Atlantic and Arctic sea–air CO₂ fluxes, 1990–2009. *Bio-*
1737 *geosciences* **10**(1): 607–627. doi:<https://doi.org/10.5194/bg-10-607-2013>.
- 1738 Shaw, WJ, Stanton, TP. 2014. Vertical diffusivity of the Western Arctic Ocean
1739 halocline. *Journal of Geophysical Research: Oceans* **119**(8): 5017–5038.
1740 doi:<https://doi.org/10.1002/2013JC009598>.
- 1741 Shibley, NC, Timmermans, ML, Carpenter, JR, Toole, JM. 2017. Spa-
1742 tial variability of the Arctic Ocean’s double-diffusive staircase.
1743 *Journal of Geophysical Research: Oceans* **122**(2): 980–994. doi:
1744 <https://doi.org/10.1002/2016JC012419>.
- 1745 Shupe, MD, Rex, M, Blomquist, B, Persson, POG, Schmale, J, Uttal, T, Althausen,
1746 D, Angot, H, Archer, S, Bariteau, L, Beck, I, Bilberry, J, Bucci, S, Buck, C,
1747 Boyer, M, Brasseur, Z, Brooks, IM, Calmer, R, Cassano, J, Castro, V, Chu, D,
1748 Costa, D, Cox, CJ, Creamean, J, Crewell, S, Dahlke, S, Damm, E, de Boer,
1749 G, Deckelmann, H, Dethloff, K, Dütsch, M, Ebell, K, Ehrlich, A, Ellis, J, En-
1750 gelmann, R, Fong, AA, Frey, MM, Gallagher, MR, Ganzeveld, L, Gradinger,

- 1751 R, Graeser, J, Greenamyre, V, Griesche, H, Griffiths, S, Hamilton, J, Heine-
1752 mann, G, Helmig, D, Herber, A, Heuzé, C, Hofer, J, Houchens, T, Howard,
1753 D, Inoue, J, Jacobi, HW, Jaiser, R, Jokinen, T, Jourdan, O, Jozef, G, King,
1754 W, Kirchgaessner, A, Klingebiel, M, Krassovski, M, Krumpfen, T, Lampert,
1755 A, Landing, W, Laurila, T, Lawrence, D, Lonardi, M, Loose, B, Lüpkes, C,
1756 Maahn, M, Macke, A, Maslowski, W, Marsay, C, Maturilli, M, Mech, M,
1757 Morris, S, Moser, M, Nicolaus, M, Ortega, P, Osborn, J, Pätzold, F, Per-
1758 ovich, DK, Petäjä, T, Pilz, C, Pirazzini, R, Posman, K, Powers, H, Pratt, KA,
1759 Preußer, A, Quéléver, L, Radenz, M, Rabe, B, Rinke, A, Sachs, T, Schulz, A,
1760 Siebert, H, Silva, T, Solomon, A, Sommerfeld, A, Spreen, G, Stephens, M,
1761 Stohl, A, Svensson, G, Uin, J, Viegas, J, Voigt, C, von der Gathen, P, Wehner,
1762 B, Welker, JM, Wendisch, M, Werner, M, Xie, Z, Yue, F. 2022. Overview
1763 of the MOSAiC expedition: Atmosphere. *Elem Sci Anth* **10**(1): 00060. doi:
1764 <https://doi.org/10.1525/elementa.2021.00060>.
- 1765 Sirevaag, A, Fer, I. 2012. Vertical heat transfer in the Arctic Ocean: The role of
1766 double-diffusive mixing. *Journal of Geophysical Research: Oceans* **117**(C7).
1767 doi:<https://doi.org/10.1029/2012JC007910>.
- 1768 Skogseth, R, McPhee, MG, Nilsen, F, Smedsrud, LH. 2013. Creation and
1769 tidal advection of a cold salinity front in Storfjorden: 1. Polynya dynam-
1770 ics. *Journal of Geophysical Research: Oceans* **118**(7): 3278–3291. doi:
1771 <https://doi.org/10.1002/jgrc.20231>.
- 1772 Smedsrud, LH, Esau, I, Ingvaldsen, RB, Eldevik, T, Haugan, PM, Li, C,
1773 Lien, VS, Olsen, A, Omar, AM, Otterå, OH, Risebrobakken, B, Sandø,
1774 AB, Semenov, VA, Sorokina, SA. 2013. The role of the Barents Sea in
1775 the Arctic climate system. *Reviews of Geophysics* **51**(3): 415–449. doi:
1776 <https://doi.org/10.1002/rog.20017>.
- 1777 Smethie Jr, W, Chipman, D, Swift, J, Koltermann, K. 1988. Chlorofluoromethanes
1778 in the Arctic Mediterranean seas: evidence for formation of bottom water
1779 in the Eurasian Basin and deep-water exchange through Fram Strait. *Deep*
1780 *Sea Research Part A Oceanographic Research Papers* **35**(3): 347–369. doi:
1781 [https://doi.org/10.1016/0198-0149\(88\)90015-5](https://doi.org/10.1016/0198-0149(88)90015-5).
- 1782 Smith, MM, Angot, H, Chamberlain, EJ, Droste, ES, Karam, S, Muilwijk, M,
1783 Webb, AL, Archer, SD, Beck, I, Blomquist, BW, Bowman, J, Boyer, M, Boz-
1784 zato, D, Chierici, M, Creamean, J, D’Angelo, A, Delille, B, Fer, I, Fong, AA,
1785 Fransson, A, Fuchs, N, Gardner, J, Granskog, MA, Hoppe, CJM, Hoppema,
1786 M, Hoppmann, M, Mock, T, Muller, S, Müller, O, Nicolaus, M, Nomura,
1787 D, Petäjä, T, Salganik, E, Schmale, J, Schmidt, K, Schulz, KM, Shupe, MD,
1788 Stefels, J, Thielke, L, Tippenhauer, S, Ulfssbo, A, van Leeuwe, M, Webster,

- 1789 M, Yoshimura, M, Zhan, L. 2023. Thin and transient meltwater layers and
1790 false bottoms in the Arctic sea ice pack—Recent insights on these histori-
1791 cally overlooked features. *Elementa: Science of the Anthropocene* **11**(1). doi:
1792 10.1525/elementa.2023.00025.
- 1793 Smith, MM, von Albedyll, L, Raphael, IA, Lange, BA, Matero, I, Salganik, E,
1794 Webster, MA, Granskog, MA, Fong, A, Lei, R, Light, B. 2022. Quantifying
1795 false bottoms and under-ice meltwater layers beneath Arctic summer sea ice
1796 with fine-scale observations. *Elementa: Science of the Anthropocene* **10**(1):
1797 000116. doi:10.1525/elementa.2021.000116.
- 1798 Snoeijs-Leijonmalm, P, Flores, H, Sakinan, S, Hildebrandt, N, Svenson,
1799 A, Castellani, G, Vane, K, Mark, FC, Heuzé, C, Tippenhauer, S,
1800 Niehoff, B, Hjelm, J, Sundberg, JH, Schaafsma, FL, Engelmann, R, The
1801 EFICA-MOSAIc Team. 2022. Unexpected fish and squid in the cen-
1802 tral Arctic deep scattering layer. *Science advances* **8**(7): eabj7536. doi:
1803 <https://doi.org/10.1126/sciadv.abj7536>.
- 1804 Somavilla, R, Schauer, U, Budéus, G. 2013. Increasing amount of Arctic Ocean
1805 deep waters in the Greenland Sea. *Geophysical Research Letters* **40**(16):
1806 4361–4366. doi:<https://doi.org/10.1002/grl.50775>.
- 1807 Son, E, Kawaguchi, Y, Cole, S, Toole, J, Ha, H. 2022. Assessment
1808 of turbulent mixing associated with eddy-wave coupling based on
1809 autonomous observations from the Arctic Canada Basin. *Journal*
1810 *of Geophysical Research: Oceans* **127**(9): e2022JC018489. doi:
1811 <https://doi.org/10.1029/2022JC018489>.
- 1812 Stanton, T, Shaw, B. 2023. Observations from Autonomous Ocean Flux Buoy 45
1813 deployed at site L3 during the MOSAIc transpolar drift, Arctic Basin, 2019-
1814 2020. Arctic Data Center. doi:10.18739/A26W96B3T.
- 1815 Stanton, TP, Shaw, WJ, Hutchings, JK. 2012. Observational study of relation-
1816 ships between incoming radiation, open water fraction, and ocean-to-ice heat
1817 flux in the Transpolar Drift: 2002–2010. *Journal of Geophysical Research:*
1818 *Oceans* **117**(C7). doi:<https://doi.org/10.1029/2011JC007871>.
- 1819 Stedmon, CA, Amon, RMW, Bauch, D, Bracher, A, Gonçalves-Araujo, R, Hopp-
1820 mann, M, Krishfield, RA, Laney, S, Rabe, B, Reader, HE, Granskog, MA.
1821 2021. Intercalibrated dataset of in situ dissolved organic matter fluorescence
1822 collected using Ice Tethered Profilers in the Central Arctic (2011-2016).
1823 PANGAEA. doi:10.1594/PANGAEA.934370.
- 1824 Stedmon, CA, Amon, RMW, Bauch, D, Bracher, A, Gonçalves-Araujo,
1825 R, Hoppmann, M, Krishfield, R, Laney, S, Rabe, B, Reader, H,
1826 Granskog, MA. 2021. Insights into water mass origins in the cen-

- 1827 tral Arctic Ocean from in-situ dissolved organic matter fluorescence.
1828 *Journal of Geophysical Research: Oceans* **126**(7): e2021JC017407. doi:
1829 <https://doi.org/10.1029/2021JC017407>.
- 1830 Steele, M, Boyd, T. 1998. Retreat of the cold halocline layer in the Arctic
1831 Ocean. *Journal of Geophysical Research: Oceans* **103**(C5): 10419–10435.
1832 doi:<https://doi.org/10.1029/98JC00580>.
- 1833 Steele, M, Morison, J, Ermold, W, Rigor, I, Ortmeier, M, Shimada,
1834 K. 2004. Circulation of summer Pacific halocline water in the Arctic
1835 Ocean. *Journal of Geophysical Research: Oceans* **109**(C2). doi:
1836 <https://doi.org/10.1029/2003JC002009>.
- 1837 Steele, M, Morley, R, Ermold, W. 2001. PHC3 Updated from: A
1838 global ocean hydrography with a high quality Arctic Ocean. *Journal
1839 of Climate* **14**(9): 2079–2087. doi:[https://doi.org/10.1175/1520-
1840 0442\(2001\)014;2079:PAGOHW;2.0.CO;2](https://doi.org/10.1175/1520-0442(2001)014;2079:PAGOHW;2.0.CO;2).
- 1841 Stroeve, J, Serreze, M, Drobot, S, Gearheard, S, Holland, M, Maslanik,
1842 J, Meier, W, Scambos, T. 2008. Arctic sea ice extent plummets in
1843 2007. *Eos, Transactions American Geophysical Union* **89**(2): 13–14. doi:
1844 <https://doi.org/10.1029/2008EO020001>.
- 1845 Takahashi, T, Sutherland, SC, Wanninkhof, R, Sweeney, C, Feely, RA, Chipman,
1846 DW, Hales, B, Friederich, G, Chavez, F, Sabine, C, Watson, A, Bakker, DCE,
1847 Schuster, U, Metzl, N, Yoshikawa-Inoue, H, Ishii, M, Midorikawa, T, No-
1848 jiri, Y, Körtzinger, A, Steinhoff, T, Hoppema, M, Olafsson, J, Arnarson, TS,
1849 Tilbrook, B, Johannessen, T, Olsen, A, Bellerby, R, Wong, CS, Delille, B,
1850 Bates, NR, de Baar, HJW. 2009. Climatological mean and decadal change in
1851 surface ocean pCO₂, and net sea–air CO₂ flux over the global oceans. *Deep
1852 Sea Research Part II: Topical Studies in Oceanography* **56**(8-10): 554–577.
1853 doi:<https://doi.org/10.1016/j.dsr2.2008.12.009>.
- 1854 Tanhua, T, Jones, EP, Jeansson, E, Jutterström, S, Smethie Jr, WM, Wallace, DW,
1855 Anderson, LG. 2009. Ventilation of the Arctic Ocean: Mean ages and inven-
1856 tories of anthropogenic CO₂ and CFC-11. *Journal of Geophysical Research:
1857 Oceans* **114**(C1). doi:<https://doi.org/10.1029/2008JC004868>.
- 1858 Terhaar, J, Lauerwald, R, Regnier, P, Gruber, N, Bopp, L. 2021. Around
1859 one third of current Arctic Ocean primary production sustained by
1860 rivers and coastal erosion. *Nature Communications* **12**(1): 169. doi:
1861 <https://doi.org/10.1038/s41467-020-20470-z>.
- 1862 Timmermans, ML, Marshall, J. 2020. Understanding Arctic Ocean circu-
1863 lation: A review of ocean dynamics in a changing climate. *Journal
1864 of Geophysical Research: Oceans* **125**(4): e2018JC014378. doi:

- 1865 <https://doi.org/10.1029/2018JC014378>.
- 1866 Timmermans, ML, Toole, JM. 2023. The Arctic Ocean's Beaufort Gyre. *Annual*
1867 *Review of Marine Science* **15**: 223–248. doi:[https://doi.org/10.1146/annurev-](https://doi.org/10.1146/annurev-marine-032122-012034)
1868 [marine-032122-012034](https://doi.org/10.1146/annurev-marine-032122-012034).
- 1869 Tippenhauer, S, Janout, M, Chouksey, M, Torres-Valdes, S, Fong, A, Wulff,
1870 T. 2021. Substantial sub-surface chlorophyll patch sustained by ver-
1871 tical nutrient fluxes in Fram Strait observed with an autonomous
1872 underwater vehicle. *Frontiers in Marine Science* **8**: 605225. doi:
1873 <https://doi.org/10.3389/fmars.2021.605225>.
- 1874 Tippenhauer, S, Vredenburg, M, Heuzé, C, Ulfsbo, A, Rabe, B, Granskog,
1875 MA, Allerholt, J, Balmonte, JP, Campbell, RG, Castellani, G, Chamber-
1876 lain, E, Creamean, J, D'Angelo, A, Dietrich, U, Droste, E, Eggers, L,
1877 Fang, YC, Fong, AA, Gardner, J, Graupner, R, Grosse, J, He, H, Hilde-
1878 brandt, N, Hoppe, CJM, Hoppmann, M, Kanzow, T, Karam, S, Koenig,
1879 Z, Kong, B, Kuhlmeiy, D, Kuznetsov, I, Lan, M, Liu, H, Mallet, M,
1880 Mohrholz, V, Muilwijk, M, Müller, O, Olsen, LM, Rember, R, Ren, J,
1881 Sakinan, S, Schaffer, J, Schmidt, K, Schuffenhauer, I, Schulz, K, Shoemaker,
1882 K, Spahic, S, Sukhikh, N, Svenson, A, Torres-Valdés, S, Torstensson,
1883 A, Wischnewski, L, Zhuang, Y. 2023a. Physical oceanography based
1884 on Ocean City CTD during POLARSTERN cruise PS122. PANGAEA. doi:
1885 <https://doi.pangaea.de/10.1594/PANGAEA.959964>.
- 1886 Tippenhauer, S, Vredenburg, M, Heuzé, C, Ulfsbo, A, Rabe, B, Granskog, MA,
1887 Allerholt, J, Balmonte, JP, Campbell, RG, Castellani, G, Chamberlain, E,
1888 Creamean, J, D'Angelo, A, Dietrich, U, Droste, E, Eggers, L, Fang, YC,
1889 Fong, AA, Gardner, J, Graupner, R, Grosse, J, He, H, Hildebrandt, N, Hoppe,
1890 CJM, Hoppmann, M, Kanzow, T, Karam, S, Koenig, Z, Kong, B, Kuhlmeiy,
1891 D, Kuznetsov, I, Lan, M, Liu, H, Mallet, M, Mohrholz, V, Muilwijk, M,
1892 Müller, O, Olsen, LM, Rember, R, Ren, J, Sakinan, S, Schaffer, J, Schmidt,
1893 K, Schuffenhauer, I, Schulz, K, Shoemaker, K, Spahic, S, Sukhikh, N, Svenson,
1894 A, Torres-Valdés, S, Torstensson, A, Wischnewski, L, Zhuang, Y. 2023b.
1895 Physical oceanography based on ship CTD during POLARSTERN cruise
1896 PS122. PANGAEA. doi:<https://doi.pangaea.de/10.1594/PANGAEA.959963>.
- 1897 Tippenhauer, S, Vredenburg, M, Heuzé, C, Ulfsbo, A, Rabe, B, Granskog,
1898 MA, Allerholt, J, Balmonte, JP, Campbell, RG, Castellani, G, Chamber-
1899 lain, E, Creamean, J, D'Angelo, A, Dietrich, U, Droste, E, Eggers, L,
1900 Fang, YC, Fong, AA, Gardner, J, Graupner, R, Grosse, J, He, H, Hilde-
1901 brandt, N, Hoppe, CJM, Hoppmann, M, Kanzow, T, Karam, S, Koenig, Z,
1902 Kong, B, Kuhlmeiy, D, Kuznetsov, I, Lan, M, Liu, H, Mallet, M, Mohrholz,

- 1903 V, Muilwijk, M, Müller, O, Olsen, LM, Rember, R, Ren, J, Sakinan,
1904 S, Schaffer, J, Schmidt, K, Schuffenhauer, I, Schulz, K, Shoemaker, K,
1905 Spahic, S, Sukhikh, N, Svenson, A, Torres-Valdés, S, Torstensson, A, Wis-
1906 chnewski, L, Zhuang, Y. 2023c. Physical oceanography water bottle samples
1907 based on ship CTD during POLARSTERN cruise PS122. PANGAEA. doi:
1908 <https://doi.pangaea.de/10.1594/PANGAEA.959965>.
- 1909 Tippenhauer, S, Vredenburg, M, Heuzé, C, Ulfsbo, A, Rabe, B, Granskog, MA,
1910 Allerholt, J, Balmonte, JP, Campbell, RG, Castellani, G, Chamberlain, E,
1911 Creamean, J, D'Angelo, A, Dietrich, U, Droste, E, Eggers, L, Fang, YC,
1912 Fong, AA, Gardner, J, Graupner, R, Grosse, J, He, H, Hildebrandt, N,
1913 Hoppe, CJM, Hoppmann, M, Kanzow, T, Karam, S, Koenig, Z, Kong, B,
1914 Kuhlmeier, D, Kuznetsov, I, Lan, M, Liu, H, Mallet, M, Mohrholz, V, Muil-
1915 wijk, M, Müller, O, Olsen, LM, Rember, R, Ren, J, Sakinan, S, Schaf-
1916 fer, J, Schmidt, K, Schuffenhauer, I, Schulz, K, Shoemaker, K, Spahic, S,
1917 Sukhikh, N, Svenson, A, Torres-Valdés, S, Torstensson, A, Wischnewski,
1918 L, Zhuang, Y. 2023d. Physical oceanography water bottle samples based
1919 on Ocean City CTD during POLARSTERN cruise PS122. PANGAEA. doi:
1920 <https://doi.pangaea.de/10.1594/PANGAEA.959966>.
- 1921 Toole, JM, Krishfield, R. 2016. Woods Hole Oceanographic Institution Ice-
1922 Tethered Profiler Program. Ice-Tethered Profiler observations: Vertical pro-
1923 files of temperature, salinity, oxygen, and ocean velocity from an Ice-
1924 Tethered Profiler buoy system. [ITP94, ITP111, Accessed March 13.
1925 2023]. NOAA National Centers for Environmental Information. doi:
1926 <https://doi.org/10.7289/v5mw2f7x>.
- 1927 Toole, JM, Krishfield, RA, Timmermans, ML, Proshutinsky, A. 2011. The ice-
1928 tethered profiler: Argo of the Arctic. *Oceanography* **24**(3): 126–135. doi:
1929 <https://doi.org/10.5670/oceanog.2011.64>.
- 1930 Torres-Valdés, S, Tsubouchi, T, Bacon, S, Naveira-Garabato, AC, Sanders, R,
1931 McLaughlin, FA, Petrie, B, Kattner, G, Azetsu-Scott, K, Whitledge, TE.
1932 2013. Export of nutrients from the Arctic Ocean. *Journal of Geophysical Re-
1933 search: Oceans* **118**(4): 1625–1644. doi:<https://doi.org/10.1002/jgrc.20063>.
- 1934 von Appen, WJ, Baumann, TM, Janout, M, Koldunov, N, Lenn, YD, Pickart,
1935 RS, Scott, RB, Wang, Q. 2022. Eddies and the distribution of eddy ki-
1936 netic energy in the Arctic Ocean. *Oceanography* **35**(3/4): 42–51. doi:
1937 <https://www.jstor.org/stable/27182695>.
- 1938 von Appen, WJ, Schauer, U, Somavilla, R, Bauerfeind, E, Beszczynska-Möller,
1939 A. 2015. Exchange of warming deep waters across Fram Strait. *Deep
1940 Sea Research Part I: Oceanographic Research Papers* **103**: 86–100. doi:

- 1941 <https://doi.org/10.1016/j.dsr.2015.06.003>.
- 1942 Wang, Q, Shu, Q, Bozec, A, Chassignet, EP, Fogli, PG, Fox-Kemper, B, Hogg,
1943 AM, Iovino, D, Kiss, AE, Koldunov, N, Le Sommer, J, Li, Y, Lin, P, Liu,
1944 H, Polyakov, I, Scholz, P, Sidorenko, D, Wang, S, Xu, X. 2023. Impact of
1945 high resolution on Arctic Ocean simulations in Ocean Model Intercompar-
1946 ison Project phase 2 (OMIP-2). *Geoscientific Model Development Discus-
1947 sions* **2023**: 1–46. doi:<https://doi.org/10.5194/gmd-2023-123>.
- 1948 Webster, MA, Holland, M, Wright, NC, Hendricks, S, Hutter, N, Itkin, P, Light, B,
1949 Linhardt, F, Perovich, DK, Raphael, IA, Smith, MM, von Albedyll, L, Zhang,
1950 J. 2022. Spatiotemporal evolution of melt ponds on Arctic sea ice: MOSAiC
1951 observations and model results. *Elementa Science of the Anthropocene* **10**(1):
1952 000072. doi:<https://doi.org/10.1525/elementa.2021.000072>.
- 1953 Zhao, M, Timmermans, ML, Cole, S, Krishfield, R, Proshutinsky, A, Toole,
1954 J. 2014. Characterizing the eddy field in the Arctic Ocean halocline.
1955 *Journal of Geophysical Research: Oceans* **119**(12): 8800–8817. doi:
1956 <https://doi.org/10.1002/2014JC010488>.
- 1957 Zweng, M, Reagan, J, Seidov, D, Boyer, T, Locarnini, R, Garcia, H, Mishonov,
1958 A, Baranova, O, Weathers, K, Paver, C, Smolyar, I. 2018. *World Ocean Atlas
1959 2018, Volume 2: Salinity*. A. Mishonov Technical Ed.; NOAA Atlas NESDIS
1960 82.